nature sustainability

Analysis

https://doi.org/10.1038/s41893-024-01358-y

Globally elevated greenhouse gas emissions from polluted urban rivers

Received: 3 October 2023

Accepted: 23 April 2024

Published online: 27 May 2024

Check for updates

Wenhao Xu $oldsymbol{0}^{1,7}$, Gongqin Wang 2,7 , Shaoda Liu $oldsymbol{0}^{1} \boxtimes$, Junfeng Wang 1 , William H. McDowell $oldsymbol{0}^{3}$, Kangning Huang $oldsymbol{0}^{4}$, Peter A. Raymond 5 , Zhifeng Yang 6 & Xinghui Xia $oldsymbol{0}^{1} \boxtimes$

Cities are at the heart of global anthropogenic greenhouse gas (GHG) emissions, with rivers embedded in urban landscapes as a potentially large yet uncharacterized GHG source. Urban rivers emit GHGs due to excess carbon and nitrogen inputs from urban environments and their watersheds. Here relying on a compiled urban river GHG dataset and robust modelling, we estimated that globally urban rivers emitted annually 1.1, 42.3 and $0.021 \,\mathrm{Tg}\,\mathrm{CH}_4$, CO_2 and $\mathrm{N}_2\mathrm{O}$, totalling $78.1 \pm 3.5 \,\mathrm{Tg}\,\mathrm{CO}_2$ -equivalent (CO_2 -eq) emissions. Predicted GHG emissions were nearly twofold those from non-urban rivers (~815 versus 414 mmol CO₂-eq m⁻² d⁻¹) and similar to scope-1 urban emissions in intensity (1,058 mmol CO_2 -eq m⁻² d⁻¹), with particularly higher CH₄ and N₂O emissions linked to widespread eutrophication and altered carbon and nutrient cycling in urban rivers. Globally, the emissions varied with national income levels with the highest emissions happening in lower-middle-income countries where river pollution control is deficient. These findings highlight the importance of pollution controls in mitigating urban river GHG emissions and ensuring urban sustainability.

More than half (-56%) of the world's population live today in urban areas and the number is projected to increase to nearly 70% by 2050¹. Urban areas harbour the highest density of human production and consumption activities. Globally, nearly 80% of gross domestic product (GDP)², 78% of final energy consumption and 70% of anthropogenic greenhouse gas (GHG) emissions³ are concentrated in urban areas, which cover <1% of the Earth's land surface⁴. Correspondingly, reducing urban GHG emissions have long been considered as a core strategy for sustainable urban development and climate change mitigation. Current urban climate change mitigation strategies target primarily anthropogenic GHG emissions from socio-economic sectors in urban areas⁵.6, but comparatively less emphasis has been placed on nature-based

mitigation pathways such as urban green–blue infrastructure because understanding of the emissions and controls is not well developed. This has hampered a comprehensive understanding of strong human–nature interactions in urban ecosystems and achieving the co-benefits of sustainable urban development and climate change mitigation.

Within cities, rivers comprise a core design component of the urban green-blue infrastructure and provide valuable socio-economic and ecological benefits to urban dwellers and wildlife⁷. Compared with less disturbed aquatic ecosystems, urban rivers are often characterized by degraded physical, chemical and biological conditions as a result of strong hydraulic regulations⁸, diffuse and point source pollutions⁹ and the urban heat island effect¹⁰ from urban areas, leading further to

¹Key Laboratory of Water and Sediment Sciences of Ministry of Education and State Key Laboratory of Water Environment Simulation, School of Environment, Beijing Normal University, Beijing, China. ²Hebei Key Laboratory of Close-to-Nature Restoration Technology of Wetlands, School of Eco-Environment, Hebei University, Baoding, China. ³Department of Natural Resources and the Environment, University of New Hampshire, Durham, NH, USA. ⁴New York University Shanghai, Shanghai, China. ⁵School of the Environment, Yale University, New Haven, CT, USA. ⁶Key Laboratory for City Cluster Environmental Safety and Green Development of the Ministry of Education, School of Ecology, Environment and Resources, Guangdong University of Technology, Guangzhou, China. ⁷These authors contributed equally: Wenhao Xu, Gongqin Wang. ⊠e-mail: liushaoda@bnu.edu.cn; xiaxh@bnu.edu.cn

disturbed elemental cycling and altered GHG emissions in urban rivers. Though evidence has been mounting that demonstrates widespread alterations to the rates $^{\rm I1-13}$ and composition $^{\rm I4}$ of GHGs (CH4, CO2 and N2O) emitted from urban rivers, most studies have been conducted at the local scale and often only consider a single GHG. For instance, studies of rivers in Asian cities $^{\rm I2,15,16}$ indicated that GHG concentrations and fluxes can be up to a dozen to 20-fold those in reference non-urban rivers. However, how do the observed local changes in urban river GHG emissions extrapolate to broader geographic scales? What are the global importance and controls of the altered urban river GHG emissions? These questions remain unanswered, highlighting a large knowledge gap in this field.

In this analysis, we presented a global synthesis of urban river GHG measurements that covered a wide range of the world's urban climatic and socio-economic conditions (Fig. 1a-d, Extended Data Fig. 7 and Supplementary Data 1). We first reviewed current urban river GHG measurements from the literature and identified distinctive patterns of GHG concentrations and fluxes in urban versus non-urban rivers. Here we considered urban rivers to be those specified as such in the original data source and non-urban rivers to be the remaining rivers, which may contain multiple river types (for example, agricultural, forested or mixed). The relationships between urban river GHG concentrations and fluxes and an array of reach-level catchment environmental and socio-economic variables were then investigated to establish machine learning-based predictive models that extrapolate our results to the global scale. We revealed two dimensions where urban river GHG emissions varied across not only a geographical but also a socio-economic gradient, which suggests non-monotonic variations with national income levels in urban river GHG emissions at the global scale. Finally, relying on global urban river extents constrained by the morphological urban areas (MUAs) of the world's cities (with 300,000 plus inhabitants)¹⁷, we found globally elevated GHG emissions and particularly higher CH₄ and N₂O emissions from urban rivers, driven by more eutrophic and anoxic aquatic conditions in these rivers. Our analysis highlights the co-benefits of restoring urban rivers in reducing both pollution and GHG emissions in urban rivers, particularly for countries that industrialize and urbanize quickly.

Results

GHG concentrations and fluxes in urban rivers

Measured CH₄, CO₂ and N₂O concentrations in urban rivers ranged from 0.01 to 311 μ mol l⁻¹, from 0.1 to 4,251 μ mol l⁻¹ and from 0.3 to 4,827 nmol l⁻¹, respectively (Fig. 1e and Supplementary Table 1). Despite the large variabilities in concentration (that is, five orders of magnitude), 100%, 95% and 94% of urban river CH₄, CO₂ and N₂O concentrations were supersaturated with respect to their atmospheric equilibria, respectively, suggesting urban rivers as sources of all three GHGs to the atmosphere. Median GHG concentrations in urban rivers were 1.3–5.0-fold those in non-urban rivers from the Global River Methane Database (GRiMeDB, canals, ditches, sites downstream of a dam or point source or affected by thermogenetic activities excluded, same below)¹⁸ (0.5 versus 0.1 μ mol l⁻¹, 90 versus 70 μ mol l⁻¹ and 38 versus 9 nmol l⁻¹ for CH₄, CO₂ and N₂O, respectively; Wilcoxon rank-sum test (same below), P < 0.001; Fig. 1e and Supplementary Table 1). These concentrations were also 1.4-3.3 times those modelled previously for global rivers, which typically did not distinguish between specific river types (mean: 4.6 versus 1.4 μmol l⁻¹, 190 versus 108–140 μmol l⁻¹ and 126 versus 39-52 nmol I⁻¹ for CH₄, CO₂ and N₂O, respectively) (Supplementary Table 2). Elevated GHG concentrations in urban rivers were furthermore substantiated by paired observations from a wide range of urban versus non-urban regional river networks (11-, 1.5- and 5-fold difference on average for CH₄, CO₂ and N₂O, respectively) (Supplementary Table 3), demonstrating systematically elevated GHG concentrations in urban rivers.

In consistency with the significantly higher concentrations, median CH₄ and N₂O fluxes in urban rivers were 4.2–4.7-fold those in non-urban rivers from GRiMeDB¹⁸ (1.4 versus 0.3 mmol m⁻² d⁻¹ and 38 versus 9 μ mol m⁻² d⁻¹ for CH₄ and N₂O, respectively, P < 0.001; Fig. 1f and Supplementary Table 1) or 1.4-41-fold those estimated previously for global rivers (mean: 11.4 versus 4.8-8.4 mmol m⁻² d⁻¹ and 203 versus 4.9-109 μmol m⁻² d⁻¹ for CH₄ and N₂O, respectively; Supplementary Table 2), suggesting significantly higher CH₄ and N₂O emissions from urban rivers. Similarly, paired measurements from urban versus non-urban (that is, agricultural, forested or mixed) regional river networks also suggested elevated CH₄ and N₂O fluxes from urban rivers (on average 17 and 10 times for CH₄ and N₂O, respectively; Supplementary Table 3 and Extended Data Fig. 1). One exception was however CO₂, for which our compiled dataset indicated slightly lower median flux than that from non-urban rivers in GRiMeDB (160 versus 195 mmol m⁻² d⁻¹, P = 0.008; Fig. 1f and Supplementary Table 1). The opposing trends in concentration (Fig. 1e) and flux (Fig. 1f) of CO₂ point to larger uncertainties associated with the CO₂ trends compared with CH₄ and N₂O (P = 0.008 versus < 0.001) and the difficulty in drawing a definitive distinction for CO₂ emissions between urban and non-urban rivers. We attribute this partially elevated trophic status (Fig. 1g) and increased in situ aquatic photosynthesis and photosynthetic uptake of CO₂ in urban rivers 14,19, though nocturnal CO₂ emissions from urban rivers is not subject to the effect²⁰. Additionally, strengthened anoxia (Fig. 1g) also favours the production of CH₄ or N₂O over CO₂ in urban rivers.

Elevated CH₄ and N₂O fluxes from urban rivers (Fig. 1f) were probably linked to enhanced nutrient and pollutant inputs from urban areas9. In particular, dissolved organic carbon and nutrient concentrations were significantly higher in urban than in non-urban rivers from GRiMeDB (P < 0.001; Fig. 1g), providing sufficient substrates (for example, reduced carbon for methanogenesis11, ammonia for nitrification²¹ and nitrate for denitrification¹³) or carbon/energy sources (for example, reduced carbon for denitrification¹³) that fuel aquatic CH₄ and N₂O production. In addition, excess organic matter inputs from untreated urban waste- or stormwater and algal bloom driven by eutrophication leads to strengthened hypoxia in slow urban river $flows ^{11,15,16} \, (Fig. \, 1g), which \, promotes \, an aerobic \, processes \, and \, provides \,$ favourable conditions for CH₄ and N₂O production in urban rivers. Though rarely investigated, the urban heat island effect is also expected to lead to increases in CH₄ and N₂O emissions from urban rivers, considering their high sensitivity to temperature^{22,23}.

Environmental and socio-economic drivers of urban river GHGs

The relationships between measured urban river GHGs and 12 catchment climatic, physical, terrestrial biospheric and socio-economic variables were explored via standardized linear regressions (Fig. 2, Extended Data Fig. 2 and Methods) to identify their macroscopic controls. The variables were computed at the reach level for entire upstream catchment of each measured urban river reach and were therefore able to account for the stream size effect in terms of the urban influences. Drainage basin area, among the 12 investigated catchment variables, showed consistent negative correlations with the concentrations and fluxes of all three GHGs (standardized linear regression coefficient (same below): -0.12 to -0.29, P = 0.002 to < 0.001) (Fig. 2), suggesting consistently higher GHG concentrations and fluxes in small embedded urban streams than in large rivers that simply flow through a city. This pattern, though not clear in similar analysis for river networks at the global scale^{24,25}, was also often reported for urban river networks at regional scales 16,26,27 and consistent with our understanding of the hierarchical nature of river networks²⁸ and the variation in importance of urban influences where small embedded urban streams often bear the strongest human influences.

In support of the above observation, computed socio-economic factors for urban river catchments also emerged as strong predictors for urban river GHG concentrations and fluxes, with larger or

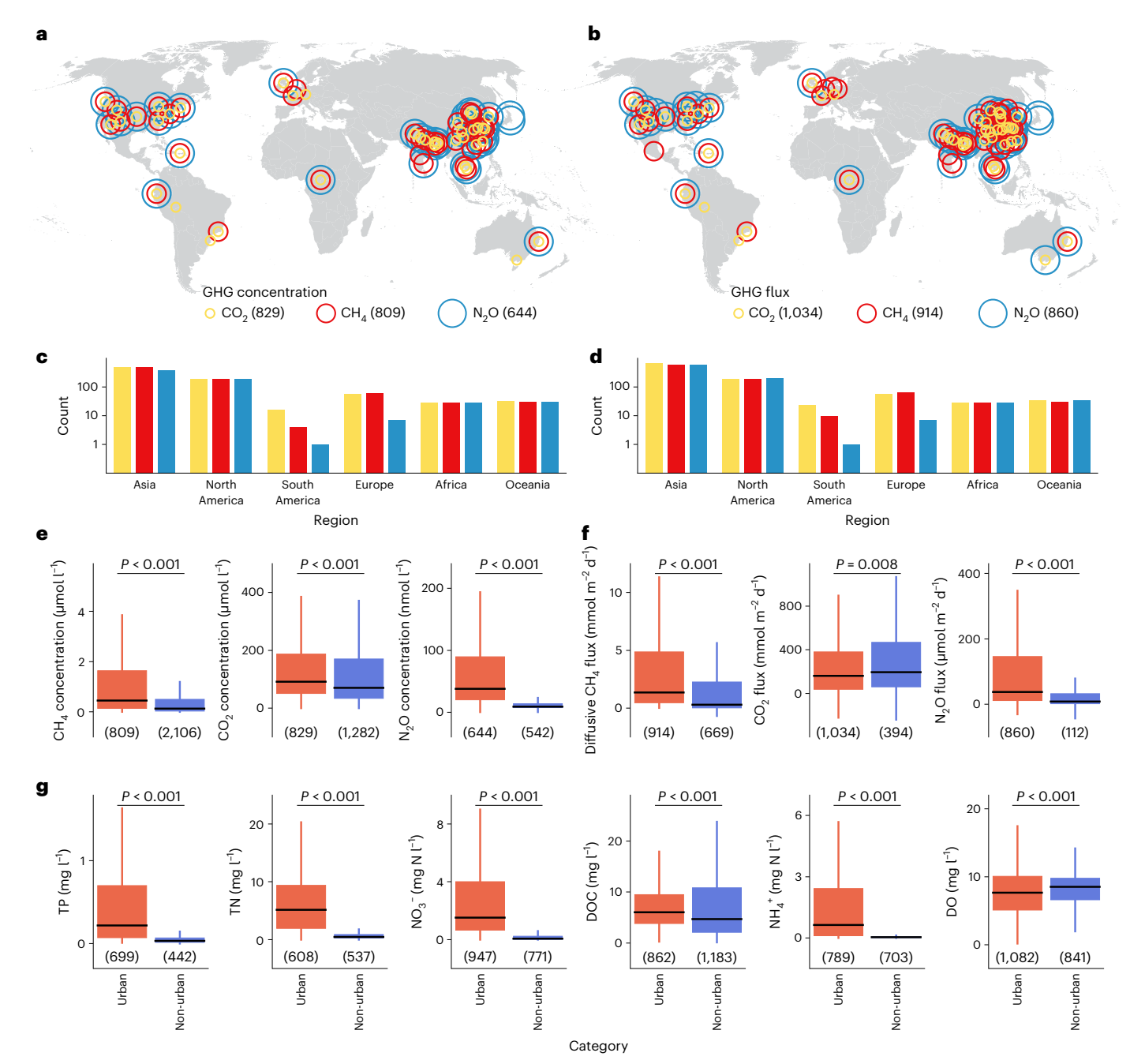


Fig. 1 | GHG concentrations and fluxes and associated physico-chemical measurements from global urban rivers. a,b, Geographical distributions of urban river GHG concentrations (a) and fluxes (b). c,d, Continental distributions of urban river GHG concentrations (c) and fluxes (d). e–g, GHG (CH₄, CO₂ and N₂O) concentrations (e), fluxes (f) and associated physico-chemical measurements (g, total phosphorous (TP), total nitrogen (TN), nitrate, dissolved organic carbon (DOC), ammonium and dissolved oxygen (DO)) in urban versus non-urban rivers from the GRiMeDB (canals, ditches, sites downstream of a dam

or point source or affected by thermogenetic activities excluded) 18 . In each plot in e-g, box spans the 25th and 75th percentiles. Solid line denotes the median and the whiskers represent 1.5× the interquartile range. Statistical significance between groups was tested with the two-sided Wilcoxon rank-sum test. Statistics also in Supplementary Table 1. Number in parentheses indicates number of measurements in a corresponding group. Basemap in a,b from GADM (https://gadm.org/).

comparable standardized coefficients than those of the rest predictors (Fig. 2). In particular, except CO_2 (which showed no clear elevations in urban rivers, Fig. 1e–f), catchment population, population density and GDP were positively correlated with the concentrations and fluxes of CH_4 (0.14–0.41, P<0.001) and N_2O (0.13–0.40, P<0.001) (Fig. 2a,d,c,f), suggesting stronger CH_4 and N_2O emissions from urban rivers in large, populated cities than in smaller urban settlements. The strong correlations were further in sharp contrast to those in similar analysis for global river networks 24,25 where catchment socio-economic factors

were only of marginal impacts, pointing to clear human influences in GHG emissions from urban rivers. The impacts of catchment GDP per capita were however negative on CH₄ and N₂O concentrations or fluxes (-0.08 to -0.09 for CH₄ and -0.07 for N₂O flux, P=0.049-0.008; Fig. 2a,d,f). Considering high sensitivity of the emissions to pollution loads in urban rivers $^{29-31}$ and reduced pollution loads to urban rivers often at the highest GDP per capita revealed by earlier studies 32,33 , we suggest a linkage between low urban river CH₄ and N₂O emissions in cities of high GDP per capita and more stringent environmental

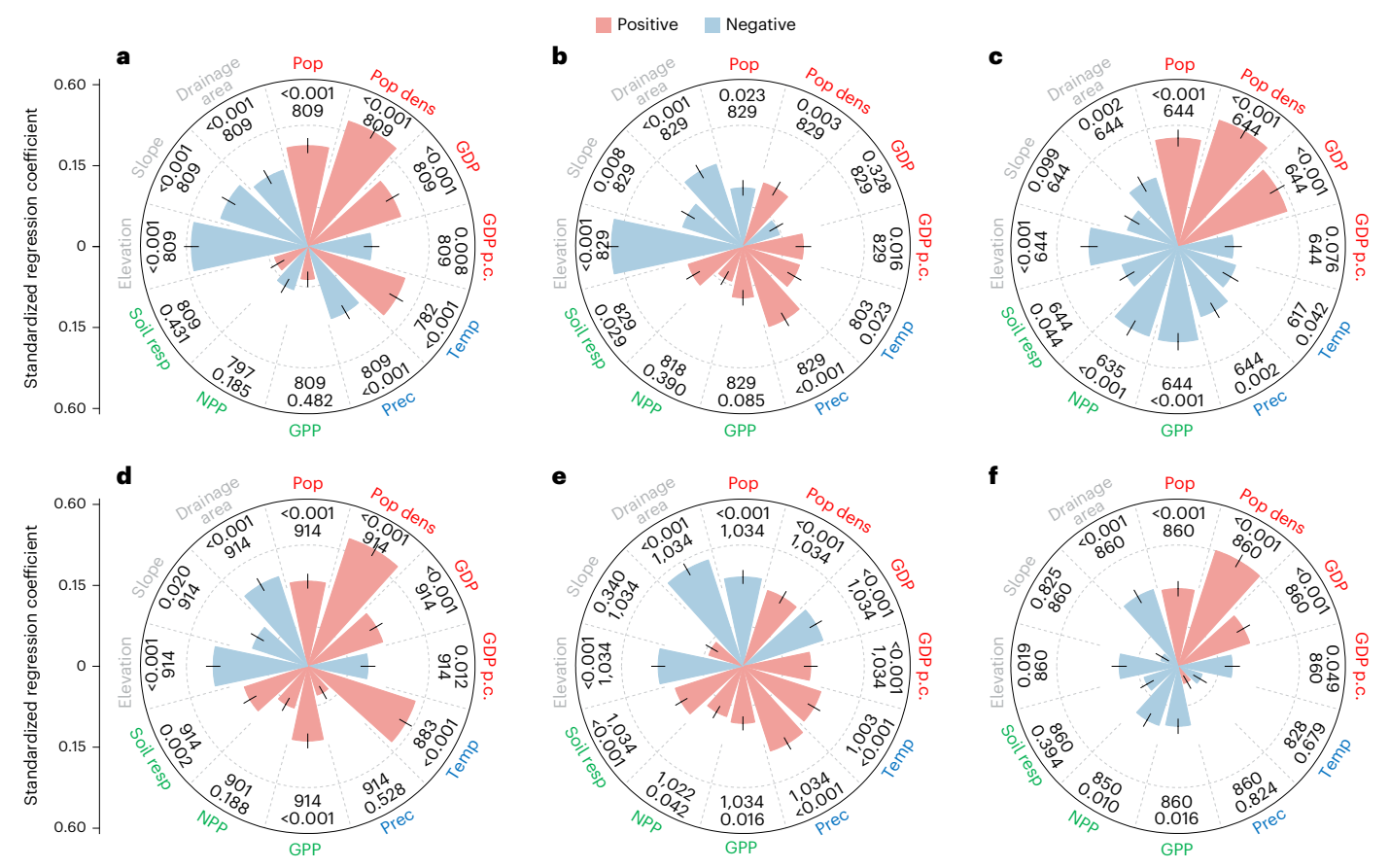


Fig. 2 | **Standardized linear regression coefficients. a-f**, Standardized linear regression coefficients between GHG concentrations (**a-c**) and fluxes (**d-f**) and 12 reach-level catchment environmental and socio-economic parameters computed for each measured urban river reach. **a,d**, CH₄. **b,e**, CO₂. **c,f**, N₂O. All dependent and independent variables were standardized using the *Z*-score normalization method (zero mean and unit standard deviation) before standardized linear regressions. Bar height corresponds to absolute value and error bar denotes standard error of the standardized regression coefficients. Bars

are colour-coded by their signs (positive or negative). Number above the bars indicates the *P* value and sample size, respectively. The *P* values were estimated with a two-sided *F*-test. No adjustments for multiple comparisons were made. Catchment variables are colour-coded by their categories (grey for physical, red for socio-economic, blue for climatic and green for terrestrial biospheric). Pop, population; Pop dens, population density; GDP p.c., gross domestic product per capita; Temp, temperature; Prec, precipitation; GPP, gross primary productivity; NPP, net primary productivity; Soil resp, soil respiration.

regulations and sewage treatments in these cities, though a full analysis is warranted for a better demonstration of the effect. Our analysis involving cities of disparate economic status therefore argues for the effectiveness of urban pollution controls in reducing GHG emissions from urban rivers.

In addition to the socio-economic influences on urban river GHGs, physical catchment properties showed strong negative correlations with urban river GHG concentrations or fluxes (Fig. 2). For instance, the concentrations and fluxes of all three GHGs were negatively correlated with catchment elevation (-0.08 to -0.40, P=0.019 to <0.001), and CH4 and CO2 concentrations were negatively correlated with catchment slope (-0.09 to -0.19, P=0.019 to <0.001; Fig. 2a,b). The observations pointed to low GHG concentrations and fluxes in urban rivers of high elevation or steep terrains, a pattern similar to those discussed for global rivers 24,25 where low in situ production or quick evasion results in low concentrations of the gases in rivers of high elevation and steep terrains.

We however point out contrasting associations between the two carbon-based (that is, CH_4 and CO_2) and the nitrogen-based (that is, N_2O) GHGs with climatic and terrestrial biospheric factors computed for urban rivers (Fig. 2). For instance, while temperature was positively correlated with CH_4 and CO_2 concentrations and fluxes (0.08-0.29, P=0.023 to <0.001; Fig. 2a,b,d,e), it was negatively correlated with N_2O concentration (-0.08, P=0.042; Fig. 2c), suggesting

low dissolved N₂O concentration in urban rivers of warmer climates (Extended Data Fig. 2). Particularly, the strong negative correlations between N₂O concentration or flux and terrestrial primary productivity (for example, GPP) or soil respiration (-0.08 to -0.21, P = 0.044 to <0.001) (Fig. 2c,f) contrasted sharply with their positive correlations with CH₄ or CO₂ fluxes in urban rivers (0.08-0.13; P = 0.042 to < 0.001;Fig. 2d,e), suggesting low N₂O concentrations and fluxes in urban rivers of high terrestrial productivity (Extended Data Fig. 2). These contrasting relationships, though together suggested strong climatic and terrestrial biospheric controls on GHGs even in highly polluted urban rivers, pointed to disparate controls of the same factors on the two groups of GHGs. We suggest that while high terrestrial ecosystem productivity or respiration support higher CH₄ or CO₂ emissions in urban rivers, as similarly suggested for global rivers^{24,25}, it on the other hand leads to greater nitrogen retention in terrestrial vegetation or soils in urban catchments^{34,35}, which inhibits surface runoff-mediated nitrogen transport to urban rivers and results in low urban river N2O concentrations in regions of high terrestrial productivity.

Global patterns of urban river GHG concentrations and fluxes

Urban river GHG concentrations and fluxes were modelled against the 12 computed reach-level catchment variables (Fig. 2) using the Random Forest (RF) regression algorithm, which accounted for multivariate interactions and nonlinearities among the variables ³⁶. The RF models

yielded reasonably good predictiveness for concentrations and fluxes of all three GHGs (R^2 = 0.60–0.72; Extended Data Figs. 3 and 9). Variable importance tests suggested that omitting one variable would result in a 3–21% increase in mean square error from the models (Extended Data Fig. 3), suggesting the importance of each variable in explaining spatial patterns of urban river GHG concentrations and fluxes. To predict urban river GHG concentrations and fluxes, the trained models were coupled with the same set of catchment predictive variables delineated for each identified urban river reach. The extent of global urban rivers was confined by the global MUAs dataset¹⁷, which covers all cities with >300,000 inhabitants on our planet (1,692 in total, re-territorialized into 1,566 MUAs; Methods).

Predicted CH_4 , CO_2 and N_2O concentrations in global urban rivers ranged from 0.9 to 40 μ mol I^{-1} , 63 to 1,029 μ mol I^{-1} and 29 to 374 nmol I^{-1} , respectively; and predicted total CH_4 , CO_2 and N_2O fluxes ranged from 3 to 124 mmol m^{-2} d^{-1} , 97 to 3,138 mmol m^{-2} d^{-1} and 23 to 842 μ mol m^{-2} d^{-1} , respectively (Fig. 3). Globally, high urban river CH_4 and CO_2 concentrations and fluxes were found in cities in India, Southeast Asia, southern China, eastern America and the tropics (Fig. 3a,b,d,e). In addition to the above places, high urban river N_2O concentrations and fluxes were also found in European, Chinese, African and South American cities (Fig. 3c,f). The slight contrast between N_2O and the two carbon-based GHGs in geographical distributions coincided with the differential climatic and terrestrial biospheric controls on the two different groups of GHGs (Fig. 2).

Here we highlight two dimensions along which urban river GHG concentrations and fluxes varied systematically. The first is a geographical dimension where urban river GHG concentrations and fluxes varied systematically along major climatic zones of Earth. In the case of CH₄ and CO₂, median concentrations and fluxes in cities of the tropics almost doubled (1.6-2.2 times) those in temperate cities (Wilcoxon rank-sum test (same below), P < 0.001; Fig. 3a,b,d,e), echoing geographical distributions of the two GHGs estimated previously for global river networks^{24,25}. In the case of N₂O, though the highest median concentration and flux were also found in the tropics, they were only 1.1–1.5 times those in temperate cities, respectively (P = 0.029)to < 0.001; Fig. 3c,f), suggesting attenuated increases in the tropics coinciding with a stronger biospheric uptake in tropical urban catchments³⁴. Nonetheless, these observations argue for strong climatic and terrestrial biospheric controls on urban river GHG emissions at the global scale even in river systems of strong human disturbances.

The second is a socio-economic dimension where urban river GHG concentrations and fluxes varied non-monotonically with national income levels (Fig. 3). In spite of the significant variations across climate zones, the concentrations and fluxes of all three GHGs increased to the highest in lower–middle-income countries (P = 0.026 to < 0.001, P = 0.100 for N₂O concentration), which then decreased monotonically to the lowest in high-income countries (P < 0.001; though still higher than the mean fluxes from global rivers³⁷, Fig. 3d-f). The same patterns remained evident when the analysis was constrained to only cities in temperate regions (Extended Data Figs. 4 and 8) where climate-induced latitudinal variations were of comparatively less importance. These inverted U-shaped relationships coincided well with the Environmental Kuznets Curve theory³⁸, which predicts pollution and environmental degradation in early stages of economic growth but reversed trend beyond some level of income per capita. For global urban river GHG emissions discussed here, we highlight severe pollutions and significantly increased emissions rates in cities in lower-middle-income countries but decreased emissions intensity in countries of higher income following more stringent pollution control39 and improved water quality40 in urban rivers.

Global GHG emissions from urban rivers

We estimated urban rivers from global cities emitted 1.1 ± 0.1 Tg CH₄ yr⁻¹ (30.4 Tg CO₂-eq (CO₂-equivalent) yr⁻¹), 42.3 ± 1.3 Tg CO₂ yr⁻¹ and

 $0.02 \pm 0.001 \,\text{Tg} \,\text{N}_2\text{O} \,\text{yr}^{-1} \,(5.4 \,\text{Tg} \,\text{CO}_2\text{-eq} \,\text{yr}^{-1})$, respectively, totalling $78.1 \pm 3.5 \,\mathrm{Tg}\,\mathrm{CO}_2$ -eq vr⁻¹ over a 100-year time horizon (same below: Fig. 4). The emissions varied between 3.5 and 10.7 Tg CO₂-eq per month after correcting for ice coverage and following enhanced emissions during ice melt at the monthly scale⁴¹ (Extended Data Figs. 5, 6 and 10). Globally, urban river GHG emissions varied over six orders of magnitude (0.01 to 1,929 Gg CO₂-eq yr⁻¹) across cities. Cities in upper-middle-income countries accounted for the largest percentage of GHG emissions from urban rivers of global cities (41.7%) (Fig. 4b) due to their largest share of the world's urban river area (50.4%) among the income groups, despite a lower mean emissions rate than the rest of global cities (674 versus 958 mmol CO₂-eq m⁻² d⁻¹). Geographically, Asian cities shared the highest percentage (66.1%) of global urban river GHG emissions (Fig. 4c) considering their overall higher emissions rate than from the rest of global cities (954 versus 635 mmol CO₂-eq m⁻² d⁻¹) and the largest share of global urban river area (56.5%) among the continents.

The emissions overall represented -1.5% of total GHG emissions estimated for global rivers (5.14 Pg CO₂-eq yr⁻¹) (ref. 37), in comparison to a share of only -0.8% by urban rivers of the total global river surface area, suggesting a nearly twofold increase compared to emissions from non-urban rivers (-815 versus 414 mmol CO₂-eq m⁻² d⁻¹). Meanwhile, the emissions represent -0.9% of the scope-1 (that is, territory- or production-based) anthropogenic CO₂ emissions from global cities (-8.6 Pg CO₂, including emissions from power, industry, ground transport, urban residential and aviation sectors)⁴². Though small, this was close to the percent urban area occupied by urban rivers in the global urban landscape (-1.2%) (ref. 17), suggesting a GHG emissions rate comparable to that of direct emissions from urban anthropogenic activities (-815 versus 1,058 mmol CO₂-eq m⁻² d⁻¹).

Importantly, the analysis identified contrasting GHG emissions profiles between urban and global rivers in general (Fig. 4d). In particular, CH₄ and N₂O made substantially higher fractions (38.9 versus 12.0% and 7.0 versus 0.7%, respectively) of the total GHG radiative forcing of urban rivers compared with global rivers³⁷, in consistency with substantially elevated CH₄ and N₂O emissions from urban rivers (Fig. 1e,f). The share of CO₂ was however substantially lower (54.2 versus 87.3%). Consequently, though covering only a small percentage of the global river surface area (-0.8%), urban rivers contributed substantially higher fractions of CH₄ and N₂O to global riverine GHG emissions in comparison to CO₂ (-4.9 and -15.4 versus - 0.9%) (ref. 37).

Discussion

Earlier efforts aiming at characterizing GHG emissions from global rivers and streams 24,25,34 often avoided (or only touched upon) systems that are highly affected by human beings. Our dedicated effort however demonstrates significantly altered GHG emissions from urban rivers in the world's cities in terms of both their emissions magnitude and intensity. We suggest incremented GHG emissions from global urban rivers (-815 minus 414, or approximately 401 mmol $\rm CO_2$ -eq m $^{-2}$ d $^{-1}$) signifies an additional anthropogenic contribution to global river GHG emissions and a direct contribution to the urban GHG budget, which requires mitigation for both a healthy urban aquatic environment and sustainable urban development.

The directional change towards stronger CH_4 and N_2O emissions in urban rivers points to a differential impact of urban anthropogenic activities on aquatic production and emission of the three GHGs, discussed also for other highly disturbed aquatic systems such as agricultural rivers⁴³ or impounded reservoirs⁴⁴. Common drivers for this change include high substrate loadings from human activities, which led to more eutrophic and reduced aquatic conditions advantageous to CH_4 and N_2O production in affected waters^{11,15,16}. CO_2 emissions from these systems is however additionally affected by enhanced in situ autotrophic activities in eutrophic urban rivers, which assimilates CO_2 via photosynthesis^{14,19}, though nocturnal emissions need to be

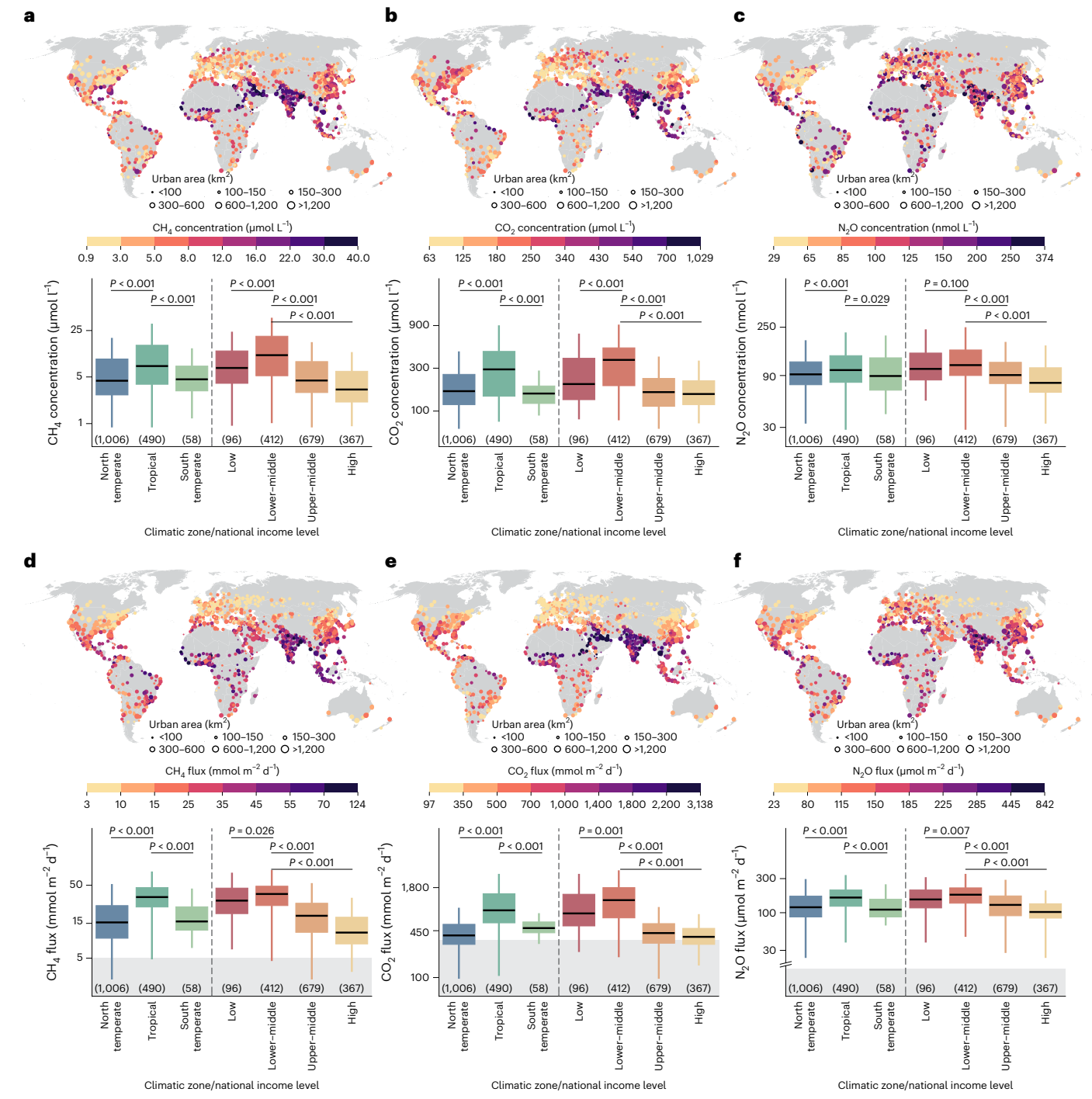


Fig. 3 | Geographical distribution of predicted GHG concentrations and fluxes in urban rivers of world's cities. $\mathbf{a}-\mathbf{f}$, Geographical distribution of predicted GHG concentrations ($\mathbf{a}-\mathbf{c}$) and fluxes ($\mathbf{d}-\mathbf{f}$) in urban rivers of world's cities. \mathbf{a},\mathbf{d} , CH₄. \mathbf{b},\mathbf{e} , CO₂. \mathbf{c},\mathbf{f} , N₂O. In each box plot, box spans the 25th and 75th percentiles. Solid line denotes the median and the whiskers represent 1.5× the interquartile range. Box plots show urban river GHG concentrations and fluxes

across different climatic zones and national income levels of world's cities. Shaded areas in sub box plots ${\bf b}, {\bf d}, {\bf f}$ indicate mean flux estimated previously for global rivers 37 . Number in parentheses indicates the number of cities in corresponding groups. Statistical significance between groups was tested with the two-sided Wilcoxon rank-sum test, using tropical and lower–middle as the reference group. Basemaps from GADM (https://gadm.org/).

monitored to correct for biases from a lack in such observations 20 . Additionally, the urban heat island effect is expected to promote CH_4 and N_2O production due to stronger temperature responses of CH_4 and N_2O than CO_2 (refs. 22,23), though further research is necessitated for a better demonstration of this effect.

Recent research highlights the effectiveness of multiple urban aquatic pollution control strategies in alleviating urban river

pollutions^{39,40,45}, with reduced GHG emissions as an additional benefit to improved water quality^{29–31}. Among these, investments on urban wastewater treatments have been demonstrated to be most effective in reducing pollution loads to urban rivers^{39,46}. In wastewater treatment plants, GHGs produced from urban wastewater treatments can be minimized by selecting the most proper processing technologies and operation parameter optimizations at much

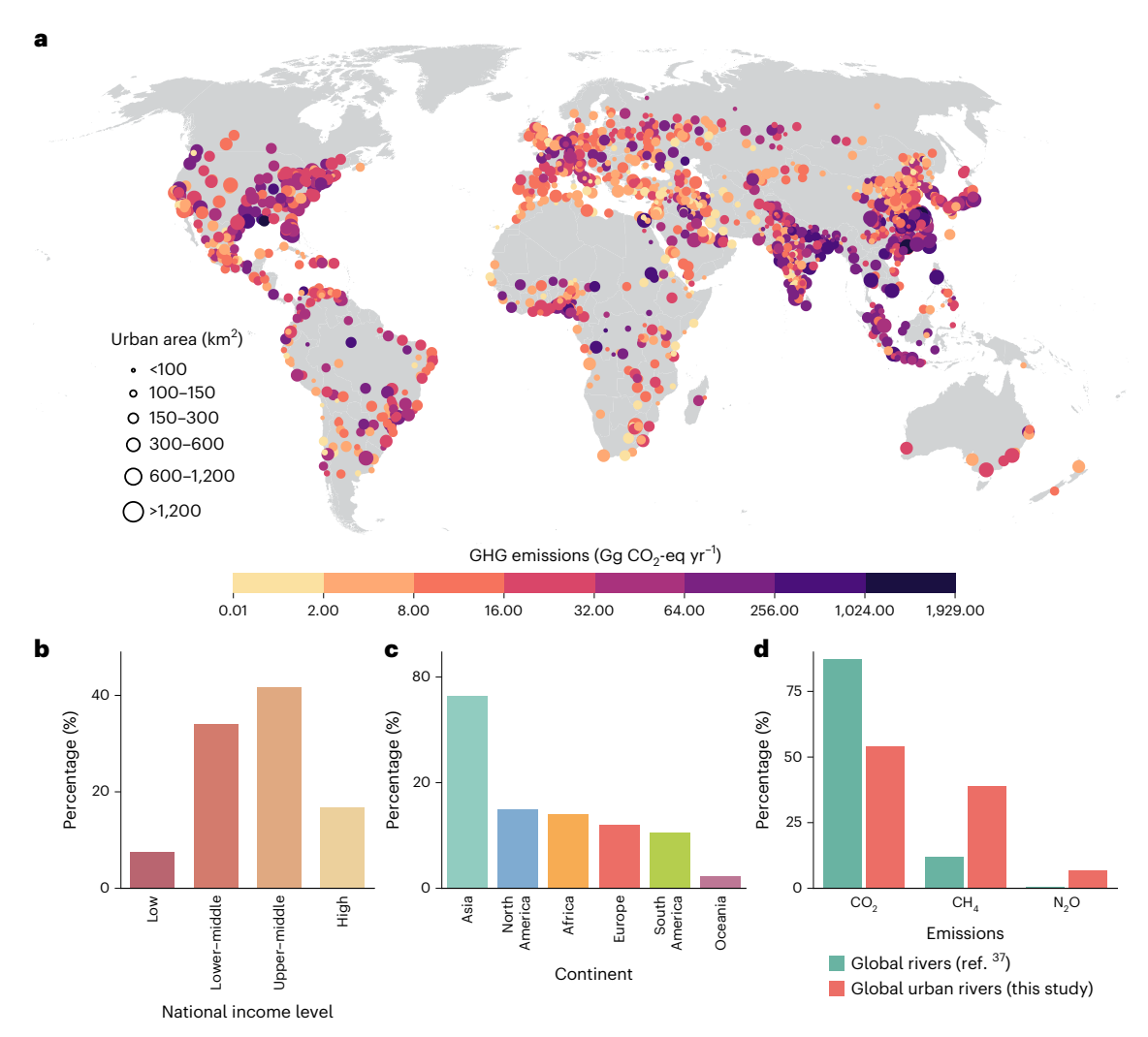


Fig. 4 | Global urban river GHG emissions in CO_2 -eq emissions. a, Geographical distribution of predicted GHG emissions in urban rivers of world's cities. b-d, Percent shares of urban river GHG emissions among the four national

income levels (**b**), six continents (**c**) and in total radiative forcing with comparison to those of global rivers (**d**), respectively. Basemap in **a** from GADM (https://gadm.org/).

lower socio-economic costs than restoring polluted urban rivers 47,48 . Additionally, CH₄ generated from wastewater treatment plants can be used for further energy or electricity production and converted to less potent CO₂ at the same time 48 . A recent example of comprehensive urban river restoration including point source elimination and sediment dredging in southern China 29 illustrates >85% reduction in CH₄ and N₂O emissions in completely restored urban rivers, with significantly lower CO₂-eq emissions and a GHG profile resembling those of non-urban rivers.

Global GHG emissions from urban rivers are expected to increase with continuous urbanization of the world in the next few decades and higher emissions rates from urban than global rivers (Fig. 3d-f). This is particularly true for low- to lower-middle-income countries located in Asia or Africa, which are projected to urbanize at a more rapid rate than the rest of the world⁴⁹. Cities in these countries face severe water quality degradation and substantial deficiencies in financial and technological support for urban water management at the same time. However, successful urban water pollution control experience from more developed countries can provide valuable reference for cities or countries that lack such experience or technological know-how. Recent nationwide improvement in surface water quality in China highlights the importance of minimizing pollution discharges from urban sectors^{40,45}. In this regard, sustained investment on urban river pollution controls and

effective international cooperation can prove invaluable in mitigating future rises in global urban river GHG emissions.

Methods

Urban river GHG dataset and global synthesis

A dataset of urban river GHG concentrations and fluxes and associated water physico-chemical properties was compiled from the literature (Supplementary Data 1 and Fig. 1). The following key terms were used to search relevant literature in Web of Science, Google Scholar and China National Knowledge Infrastructure: Topics = ('Carbon dioxide*' OR 'Methane*' OR 'Nitrous oxide*' OR 'CO2*' OR 'CH4*' OR 'N2O*' OR 'Greenhouse gas*' OR 'GHG emission*') and ('River*' OR 'Stream*' OR 'Inland water*' OR 'Freshwater*') and ('City*' OR 'Urban*' OR 'Urbanized area*' OR 'Land use*'). We retained only studies that report in situ measurements of urban river GHG concentrations or fluxes. For papers that had a concentration reported, corresponding diffusive flux was estimated following Fick's Law using local water physico-chemical parameters as drivers. For studies that have measurements from both urban and non-urban river segments, both types were retained for comparative analysis (Supplementary Table 3). We also kept the database strictly spatially explicit so that exact geographical locations of the measurement sites can be determined. All data were either extracted directly from text and tables or digitized from figures with the support

of GetData Graph Digitizer (version 2.22) from the original papers. In total, 5.090 individual urban river GHG concentration and flux measurements were recorded, which covered all major climatic zones of the world (Fig. 1a-d). Though with a more concentrated distribution in Asia and North America, this dataset covered a wide range (94–99%) of the world's urban climatic (mean annual temperature: 5.8-28.6 °C, mean annual precipitation: 233-2,835 mm yr⁻¹) and socio-economic (GDP per capita, US\$500-160,000; MUA population, 79,000 to >40,000,000) conditions (Extended Data Fig. 7) and was therefore concluded to be representative of urban river GHG emissions. Total numbers of measurements were 829, 809 and 644 for CO₂, CH₄ and N₂O concentrations, respectively, and 1,034, 914, 860 for CO₂, CH₄ and N₂O fluxes, respectively. Related physico-chemical measurements were also recorded, which included concentrations for nitrate, ammonium, total nitrogen (TN), total phosphorus (TP), dissolved oxygen (DO), dissolved organic carbon (DOC), chlorophyll a, total carbon, total organic carbon, pH, wind speed and flow velocity.

Urban boundary dataset

In this analysis, the global Morphological Urban Areas (MUA) dataset was used as a boundary for defining urban river extents. The dataset is a re-territorialized product based on the remote sensing-based high-resolution Global Urban Footprint datasets and provides consistent descriptions of the world's major morphologically contiguous urban areas/agglomerations. The dataset covers 1,692 cities with >300,000 residents on the planet, which are aggregated into 1,566 separate MUAs that are geographically near urban areas (for example, the largest MUA is Pearl River Delta including Guangzhou, Shenzhen, Dongguan and so on as one urban agglomeration). Besides providing boundaries for the world's major urban areas/agglomerations, the dataset also provides additional characteristics of the urban areas including surface area and population. We however note conservativeness in our global urban river GHG estimates considering global MUAs do not cover smaller urban settlements.

The world's urban river extents were determined by overlapping global MUAs with the Global Reach-Level A Priori Discharge Estimates for Surface Water and Ocean Topography (GRADES) river networks of Surface Water and Ocean Topography (GRADES) river networks which is vectorized global river network product that contains allilion individual river reaches. GRADES river reaches that fall within the boundary of MUAs were defined as urban rivers and formed target of the current analysis. The GRADES dataset further provides daily discharge estimates for years 1979–2014, from which multi-year mean monthly discharges were derived and used to calculate monthly urban river surface area and gas transfer velocities for urban river GHG emissions.

The World Bank groups the world's 215 countries and economies into four major income groups (low, lower-middle, upper-middle and high) based on gross national income per capita (Extended Data Fig. 8)⁵². To explore the impacts of a country's socio-economic development level on urban river GHG emissions, all MUAs were classified into four economic groups according to income levels of the country they reside in. According to the results, 96 of the global MUAs reside in low-income countries, 412 in lower-middle-income countries, 679 in upper-middle-income countries and 367 MUAs reside in high-income countries.

Urban river GHG modelling

To model urban river GHG concentrations and fluxes, 12 reach-level catchment environmental and socio-economic predictors were calculated for entire upstream catchment of each identified urban river reach. Catchment corresponding an urban river reach was determined by identifying all upstream reaches (and associated sub-catchments) utilizing topological relationships provided by the GRADES river network dataset. Catchment predictors were then calculated by overlapping the catchments with relevant geospatial datasets

(Supplementary Table 4 provides detailed source information of the geospatial datasets) using the mask tool of the Python Rasterio toolsets (version 1.4). Depending on property of a predicting variable, either sum or arithmetic mean of all grid cells that fall within the delineated drainage basin was calculated.

Calculated catchment predictors included two climatic variables (temperature and precipitation), three terrestrial biospheric variables (gross primary productivity, net primary productivity, soil respiration rate), three geomorphic variables (catchment area, elevation and slope) and four socio-economic indicators (population density, GDP, population, GDP per capita). Among the 12 predicting variables, temperature, precipitation, soil respiration rate, gross primary productivity and net primary productivity had monthly values that could be matched to individual GHG concentration and flux measurements from the compiled urban river GHG dataset.

We applied a standardized linear regression model⁵³ to explore the effects of different environmental and socio-economic predictors on urban river GHG concentrations or fluxes considering its straightforwardness in illustrating the effects. GHG concentrations and fluxes and corresponding predictable variables were log-transformed if they were non-normally distributed. All independent and dependent variables were then *Z*-score normalized before linear regression so that all variables had a zero mean and a standard deviation of one. The standardized regression coefficients were used for inter-comparisons for the effects of different catchment predictors on urban river GHG concentrations or fluxes. A positive coefficient indicates a positive impact (vice versa) and the magnitude of coefficient scales with importance of the impact.

The RF regression model (randomForest package in R, version 4.2.1), a well-established machine learning algorithm, was used for quantitative modelling of urban river GHG concentrations and fluxes. We used all of the 12 collated catchment variables as predictors considering the RF algorithm's capacity to randomly select variables for modelling and that the algorithm was not affected by nonlinearity or interactions among the variables³⁶. For modelling, 85% of the GHG concentration or flux records were randomly chosen for training and the rest for model performance evaluation. The number of predictive variables to use in each split (mtry) and the number of trees (ntree) were set to be 5 and 500, respectively. The model yielded reasonably good predictiveness for GHG concentrations and fluxes ($R^2 = 0.60 - 0.72$) (Extended Data Fig. 3a-f), Furthermore, the modelling framework also yielded reasonably good seasonal GHG concentrations and fluxes $(R^2 = 0.45 - 0.86;$ Extended Data Fig. 9). To estimate ebullitive CH₄ flux from urban rivers, the linear relationship between ebullitive and diffusive CH₄ flux developed in ref. 25 was used.

Emissions upscaling

To predict urban river GHG emissions, the trained flux models were coupled with reach-level catchment variables calculated for all identified urban river reaches. Among the predicting variables, temperature, precipitation, soil respiration, gross primary productivity and net primary productivity were monthly resolved, which allowed for calculations of monthly river GHG fluxes. The emissions fluxes were then coupled with monthly resolved, reach-level river surface area calculated following ref. 24. Briefly, the monthly river surface area product was based on the GRADES river networks, where monthly widths of a reach were estimated by coupling downstream and at-a-station hydraulic geometries with reach-level monthly discharge estimates from GRADES. Total river surface area within an urban area included additional surface area for the smallest rivers not represented by the GRADES hydrography dataset (GRADES starts its channelization at a catchment area of ~25 km²). This part of surface area was also provided by ref. 24 and estimated by extrapolating existing reach-level GRADES surface area using scaling relationships with Strahler stream order. The extrapolated area was resolved at a HydroBASIN 04 level²⁴ and at a

monthly scale, which was downscaled to each MUA for use in emissions estimates in this analysis.

Given the wide geographical distribution of global MUAs, seasonal ice coverage needs to be considered for river GHG emissions at the annual scale. The duration of ice-free days was roughly estimated using monthly air temperature at the monthly scale (Extended Data Fig. 5). We conservatively assumed that urban rivers were ice covered and do not exchange gases with the atmosphere when air temperature was below -2 °C. Then, annual GHG emissions from urban rivers of an MUA were calculated by summing up emissions from all ice-free months. We further applied a correction for enhanced emissions during ice melting periods due to the release of GHGs produced and built up subsurface over the winter. This correction was done on the annual basis following ref. 41 where authors reported that GHGs released during ice melting periods made up ~17% and 27% of annual CO₂ and CH₄ emissions, respectively. Though data were insufficient, preliminary evidence⁵⁴ suggests that similar subsurface processes exist for N₂O. We therefore applied a ratio of 17% (same as that for CO₂) for correcting for enhanced N₂O emissions from ice melting. The effects of accounting for the ice-cover and ice melting corrections for GHG emissions were illustrated on a latitudinal gradient (Extended Data Fig. 5) and for individual months (Extended Data Fig. 6). To report total emissions and account for global warming potentials (over a 100-year time horizon)⁵⁵ of the three GHGs, the CO₂-equivalent emissions were also calculated using conversation ratios of 27 and 273 for CH₄ and N₂O, respectively.

Uncertainty analysis

Uncertainties associated with urban river GHG emissions estimates were determined using the Monte Carlo simulation method. The simulations were conducted using the rnorm function of R (version 4.2.1). Two major error sources were considered: error associated with predicted GHG fluxes from the RF models and error associated with our reach-level river surface area estimates. The RF model residuals were fitted to a normal distribution (Extended Data Fig. 10a-c), and errors at one standard deviation were determined to be 0.46, 0.18 and 0.30 in terms of log base 10 values for CH₄, CO₂ and N₂O flux, respectively. For reach-level surface area, we compared with those from the Global River Widths from Landsat (GRWL) database⁵⁶. The error at one standard deviation was determined to be 0.35 or ~8.9% of the mean reach-level surface area in log base 10 values (m²) (Extended Data Fig. 10d). The error ranges defined above were propagated through the predicting processes for each GHG for 1.000 times. Final distributions of GHG emissions from the Monte Carlo simulations were used to calculate standard errors associated with the urban river GHG emissions estimates.

Reporting summary

Further information on research design is available in the Nature Portfolio Reporting Summary linked to this article.

Data availability

The global morphological urban areas product is available from https://data.mendeley.com/datasets/v3p8gk5724/1. The Global Reach-scale A priori Discharge Estimates for SWOT (GRADES) dataset is available from https://www.reachhydro.org/home/records/grades. The Global River Methane Database (GriMeDB) is available from https://doi.org/10.6073/pasta/f48cdb77282598052349e969920356ef. The temperature and precipitation are available from WorldClim (version 2) (https://www.worldclim.org/data/worldclim21.html). The elevation and slope are available from Global Multi-resolution Terrain Elevation Dataset (https://www.earthenv.org/topography). The GDP and GDP per capita are available from Gridded global datasets for Gross Domestic Product and Human Development Index over 1990–2015 via Dryad at https://doi.org/10.5061/dryad.dklj0 (ref. 57). The population density is available from Gridded Population of the World (version 4)

(https://beta.sedac.ciesin.columbia.edu/data/set/gpw-v4-population-density). The MODIS gross and net primary productivity data are available from https://www.umt.edu/numerical-terradynamic-simulation-group/project/modis/mod17.php. The soil respiration rates data are available from http://cse.ffpri.affrc.go.jp/shojih/data/index. html. Detailed information on an array of spatially explicit geospatial datasets used in this analysis is summarized in Supplementary Table 4. The dataset of urban river GHG concentrations and fluxes and related physico-chemical properties is available via figshare at https://doi.org/10.6084/m9.figshare.24233902 (ref. 58). Source data are provided with this paper.

Code availability

All data processing and analysis were performed using Microsoft Excel (version 2021), OriginPro (version 2023), randomForest package in R (version 4.2.1) and ArcGIS (version 10.8). The code used in this study is available via figshare at https://doi.org/10.6084/m9.figshare.24233902 (ref. 58).

References

- World Cities Report 2022: Envisaging the Future of Cities (UN-Habitat, 2022).
- 2. Urban Development (World Bank, 2023).
- 3. Urban Climate Action—The Urban Content of the NDCs: Global Review 2022 (UN-Habitat, 2022).
- Liu, Z., He, C., Zhou, Y. & Wu, J. How much of the world's land has been urbanized, really? A hierarchical framework for avoiding confusion. *Landscape Ecol.* 29, 763–771 (2014).
- 5. Creutzig, F. et al. Global typology of urban energy use and potentials for an urbanization mitigation wedge. *Proc. Natl Acad. Sci. USA* **112**, 6283–6288 (2015).
- Ramaswami, A. et al. Carbon analytics for net-zero emissions sustainable cities. Nat. Sustain. 4, 460–463 (2021).
- 7. Perini, K. & Sabbion, P. Urban Sustainability and River Restoration: Green and Blue Infrastructure (John Wiley & Sons, 2016).
- 8. Gurnell, A., Lee, M. & Souch, C. Urban rivers: hydrology, geomorphology, ecology and opportunities for change. *Geogr. Compass* **1**, 1118–1137 (2007).
- Strokal, M. et al. Urbanization: an increasing source of multiple pollutants to rivers in the 21st century. npj Urban Sustain. 1, 24 (2021).
- Peng, S. S. et al. Surface urban heat island across 419 global big cities. Environ. Sci. Technol. 46, 696–703 (2012).
- Wang, G. Q. et al. Intense methane ebullition from urban inland waters and its significant contribution to greenhouse gas emissions. Water Res. 189, 116654 (2021).
- Wang, X. F. et al. pCO₂ and CO₂ fluxes of the metropolitan river network in relation to the urbanization of Chongqing, China. J. Geophys. Res. 122, 470–486 (2017).
- Song, K. et al. Distinctive microbial processes and controlling factors related to indirect N₂O emission from agricultural and urban rivers in Taihu watershed. *Environ. Sci. Technol.* 56, 4642–4654 (2022).
- Wang, G. Q. et al. Unexpected low CO₂ emission from highly disturbed urban inland waters. *Environ. Res.* 235, 116689 (2023).
- 15. Zhang, W. S. et al. Urban rivers are hotspots of riverine greenhouse gas (N_2O , CH_4 , CO_2) emissions in the mixed-landscape Chaohu Lake basin. *Water Res.* **189**, 116624 (2021).
- 16. Yu, Z. J. et al. Carbon dioxide and methane dynamics in a human-dominated lowland coastal river network (Shanghai, China). *J. Geophys. Res.* **122**, 1738–1758 (2017).
- Taubenböck, H. et al. A new ranking of the world's largest cities do administrative units obscure morphological realities? *Remote Sens. Environ.* 232, 111353 (2019).

- Stanley, E. H. et al. GriMeDB: the global river database of methane concentrations and fluxes. *Earth Syst. Sci. Data* 15, 2879–2926 (2022).
- 19. Ran, L. S. et al. Substantial decrease in CO_2 emissions from Chinese inland waters due to global change. *Nat. Commun.* **12**, 1730 (2021).
- Gómez-Gener, L. et al. Global carbon dioxide efflux from rivers enhanced by high nocturnal emissions. *Nat. Geosci.* 14, 289–294 (2021).
- Garnier, J. et al. Nitrous oxide (N₂O) in the Seine River and basin: observations and budgets. Agric. Ecosyst. Environ. 133, 223–233 (2009).
- 22. Yvon-Durocher, G. et al. Methane fluxes show consistent temperature dependence across microbial to ecosystem scales. *Nature* **507**, 488–491 (2014).
- 23. Velthuis, M. & Veraart, A. J. Temperature sensitivity of freshwater denitrification and N_2O emission—a meta-analysis. *Glob. Biogeochem. Cycles* **36**, e2022GB007339 (2022).
- Liu, S. D. et al. The importance of hydrology in routing terrestrial carbon to the atmosphere via global streams and rivers. *Proc. Natl Acad. Sci. USA* 119, e2106322119 (2022).
- Rocher-Ros, G. et al. Global methane emissions from rivers and streams. Nature 621, 530–535 (2023).
- Smith, R. M. et al. Influence of infrastructure on water quality and greenhouse gas dynamics in urban streams. *Biogeosciences* 14, 2831–2849 (2017).
- Tang, W. et al. Land use and hydrological factors control concentrations and diffusive fluxes of riverine dissolved carbon dioxide and methane in low-order streams. Water Res. 231, 119615 (2023).
- Da Costa, F. P., Grinfeld, M. & Wattis, J. A. D. A hierarchical cluster system based on Horton–Strahler rules for river networks. Stud. Appl. Math. 109, 163–204 (2002).
- Wang, X. F. et al. Methane and nitrous oxide concentrations and fluxes from heavily polluted urban streams: comprehensive influence of pollution and restoration. *Environ. Pollut.* 313, 120098 (2022).
- 30. Wang, J. L. et al. Ecological restoration effectively mitigated pCO_2 and CO_2 evasions from severely polluted urban rivers. *J. Geophys. Res.* **128**, e2023JG007531 (2023).
- Yan, R. F. et al. Pollution abatement reducing the river N₂O emissions although it is partially offset by a warming climate: insights from an urbanized watershed study. Water Res. 236, 119934 (2023).
- 32. Zhang, X. et al. Managing nitrogen for sustainable development. *Nature* **528**, 51–59 (2015).
- Zhou, W. L. et al. Water environment protection and sustainable development in townlet of China: a case study in Taicang. J. Environ. Sci. 110, 129–139 (2021).
- Yao, H. Z. et al. Increased global nitrous oxide emissions from streams and rivers in the Anthropocene. Nat. Clim. Change 10, 138–142 (2020).
- Lucas, R. W. et al. Long-term declines in stream and river inorganic nitrogen export correspond to forest change. *Ecol. Appl.* 26, 545–556 (2016).
- 36. Breiman, L. Random forests. Mach. Learn. 45, 5-32 (2001).
- Lauerwald, R. et al. Inland water greenhouse gas budgets for RECCAP2: 2. regionalization and homogenization of estimates. Glob. Biogeochem. Cycles 37, e2022GB007658 (2023).
- 38. Grossman, G. M. & Krueger, A. Economic growth and the environment. Q. J. Econ. **110**, 353–377 (1995).
- 39. Xu, Z. X. et al. Urban river pollution control in developing countries. *Nat. Sustain.* **2**, 158–160 (2019).
- Ma, T. et al. China's improving inland surface water quality since 2003. Sci. Adv. 6, eaau3798 (2020).

- Denfeld, B. A. et al. A synthesis of carbon dioxide and methane dynamics during the ice-covered period of northern lakes. *Limnol. Oceanogr. Lett.* 3, 117–131 (2018).
- 42. Huo, D. et al. Carbon monitor cities near-real-time daily estimates of CO₂ emissions from 1,500 cities worldwide. *Sci. Data* **9**, 533 (2022).
- 43. Wu, W. X. et al. Agricultural ditches are hotspots of greenhouse gas emissions controlled by nutrient input. *Water Res.* **242**, 120271 (2023).
- 44. Soued, C. et al. Reservoir CO₂ and CH₄ emissions and their climate impact over the period 1900–2060. *Nat. Geosci.* **15**, 700–705 (2022).
- 45. Yu, C. Q. et al. Managing nitrogen to restore water quality in China. *Nature* **567**, 516–520 (2019).
- Lund, N. S. V. et al. Integrated stormwater inflow control for sewers and green structures in urban landscapes. *Nat. Sustain.* 2, 1003–1010 (2019).
- Campos, J. L. et al. Greenhouse gases emissions from wastewater treatment plants: minimization, treatment, and prevention.
 J. Chem. 2016, 3796352 (2016).
- 48. Keller, J. & Hartley, K. Greenhouse gas production in wastewater treatment: process selection is the major factor. *Water Sci. Technol.* 47, 43–48 (2003).
- 49. Montgomery, M. R. The urban transformation of the developing world. Science **319**, 761–764 (2008).
- 50. Esch, T. et al. Where we live—a summary of the achievements and planned evolution of the global urban footprint. *Remote Sens.* **10**, 895 (2018).
- 51. Lin, P. R. et al. Global reconstruction of naturalized river flows at 2.94 million reaches. *Water Resour. Res.* **55**, 6499–6516 (2019).
- 52. World Development Indicators (World Bank, 2021).
- 53. Schielzeth, H. Simple means to improve the interpretability of regression coefficients. *Methods Ecol. Evol.* 1, 103–113 (2010).
- Cavaliere, E. & Baulch, H. M. Denitrification under lake ice. Biogeochemistry 137, 285–295 (2018).
- 55. Forster, P. et al. in *Climate Change 2021: The Physical Science Basis* (eds Masson-Delmotte, V. et al.) 923–1054 (Cambridge Univ. Press, 2021).
- 56. Allen, G. H. & Pavelsky, T. M. Global extent of rivers and streams. Science **361**, 585–588 (2018).
- 57. Kummu, M., Maija, T. & Guillaume, J. H. A. Data from: gridded global datasets for gross domestic product and human development index over 1990–2015. *Dryad* https://doi.org/10.5061/dryad.dk1j0 (2020).
- 58. Xu, W. H. et al. Urban river GHG dataset. figshare https://doi.org/10.6084/m9.figshare.24233902 (2024).

Acknowledgements

This work was supported by the National Natural Science Foundation of China (T2261129474 (X.X.), 52388101 (Z.Y.), 52039001 (X.X.) and 52379057 (S.L.)), the National Key Research and Development Project of China (2021YFC3200401 (S.L.)) and the US National Science Foundation (2215300 (W.H.M.)).

Author contributions

X.X. and S.L. designed the study. W.X. and G.W. compiled and analysed the data. J.W. aided in the analysis and compilation of the dataset. X.X., S.L., W.X., G.W. and J.W. interpreted the results and wrote the first draft of the paper. W.H.M., K.H., P.A.R. and Z.Y. provided insights and revised the paper. All authors contributed to the discussion and revision of the paper.

Competing interests

The authors declare no competing interests.

Additional information

Extended data is available for this paper at https://doi.org/10.1038/s41893-024-01358-y.

Supplementary information The online version contains supplementary material available at https://doi.org/10.1038/s41893-024-01358-y.

Correspondence and requests for materials should be addressed to Shaoda Liu or Xinghui Xia.

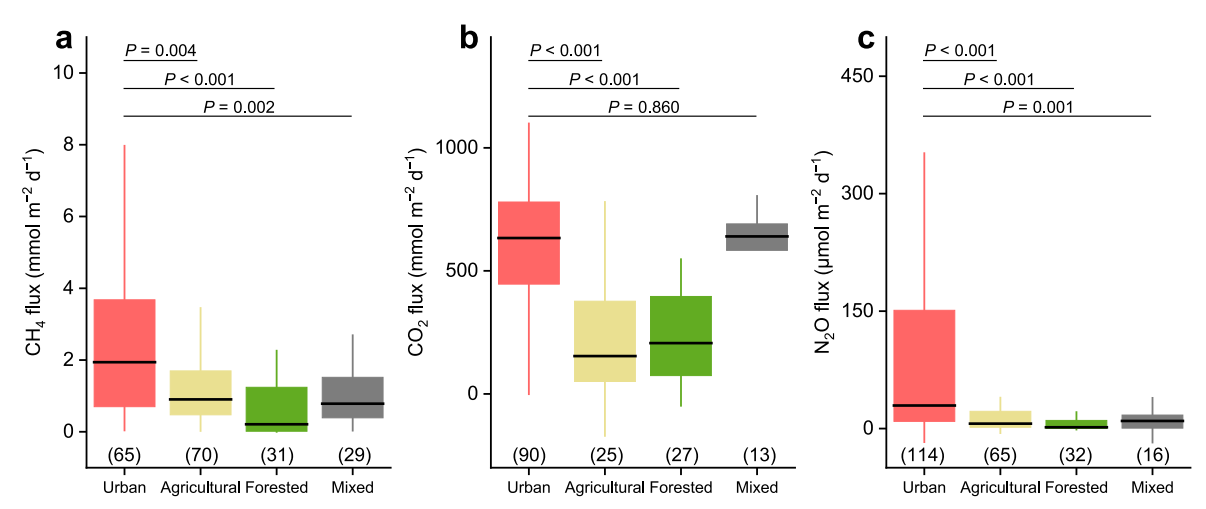
Peer review information *Nature Sustainability* thanks Alberto Borges and the other, anonymous, reviewer(s) for their contribution to the peer review of this work.

Reprints and permissions information is available at www.nature.com/reprints.

Publisher's note Springer Nature remains neutral with regard to jurisdictional claims in published maps and institutional affiliations.

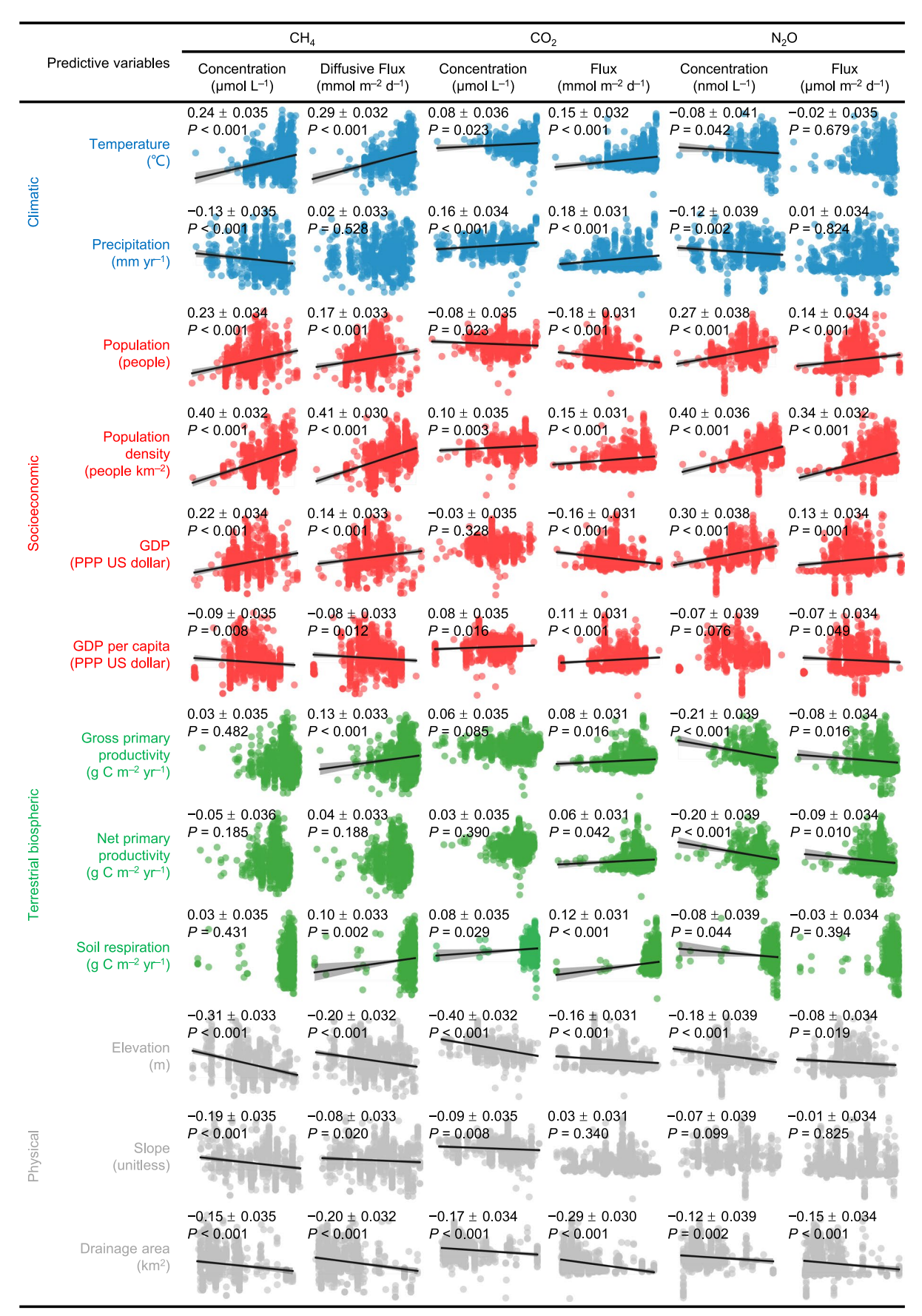
Springer Nature or its licensor (e.g. a society or other partner) holds exclusive rights to this article under a publishing agreement with the author(s) or other rightsholder(s); author self-archiving of the accepted manuscript version of this article is solely governed by the terms of such publishing agreement and applicable law.

© The Author(s), under exclusive licence to Springer Nature Limited 2024



Extended Data Fig. 1 | Comparing measured GHG emission fluxes between urban rivers and other river types from the compiled urban river GHG dataset. a, CH_4 flux. b, CO_2 flux. c, N_2O flux. ln each plot, box spans the 25th and 75th percentiles. Solid line denotes the median and the whiskers represent

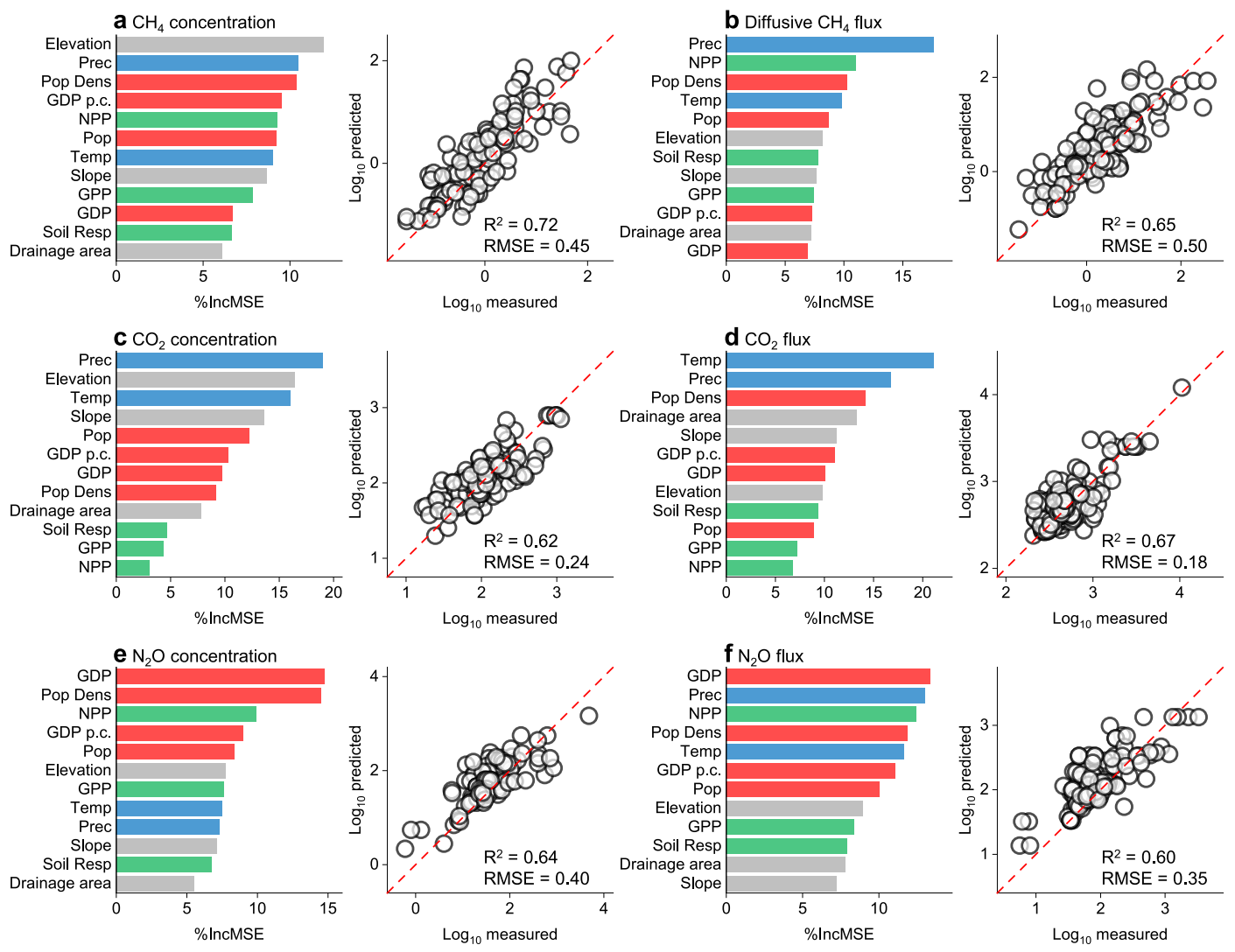
 $1.5 \times$ the interquartile range. Statistical significance between groups was tested with the two-sided Wilcoxon rank-sum test, using urban river as the reference group. Number in parentheses indicates number of measurements.



Extended Data Fig. 2 | Relationships between urban river GHG concentrations and fluxes and catchment environmental and socioeconomic variables.

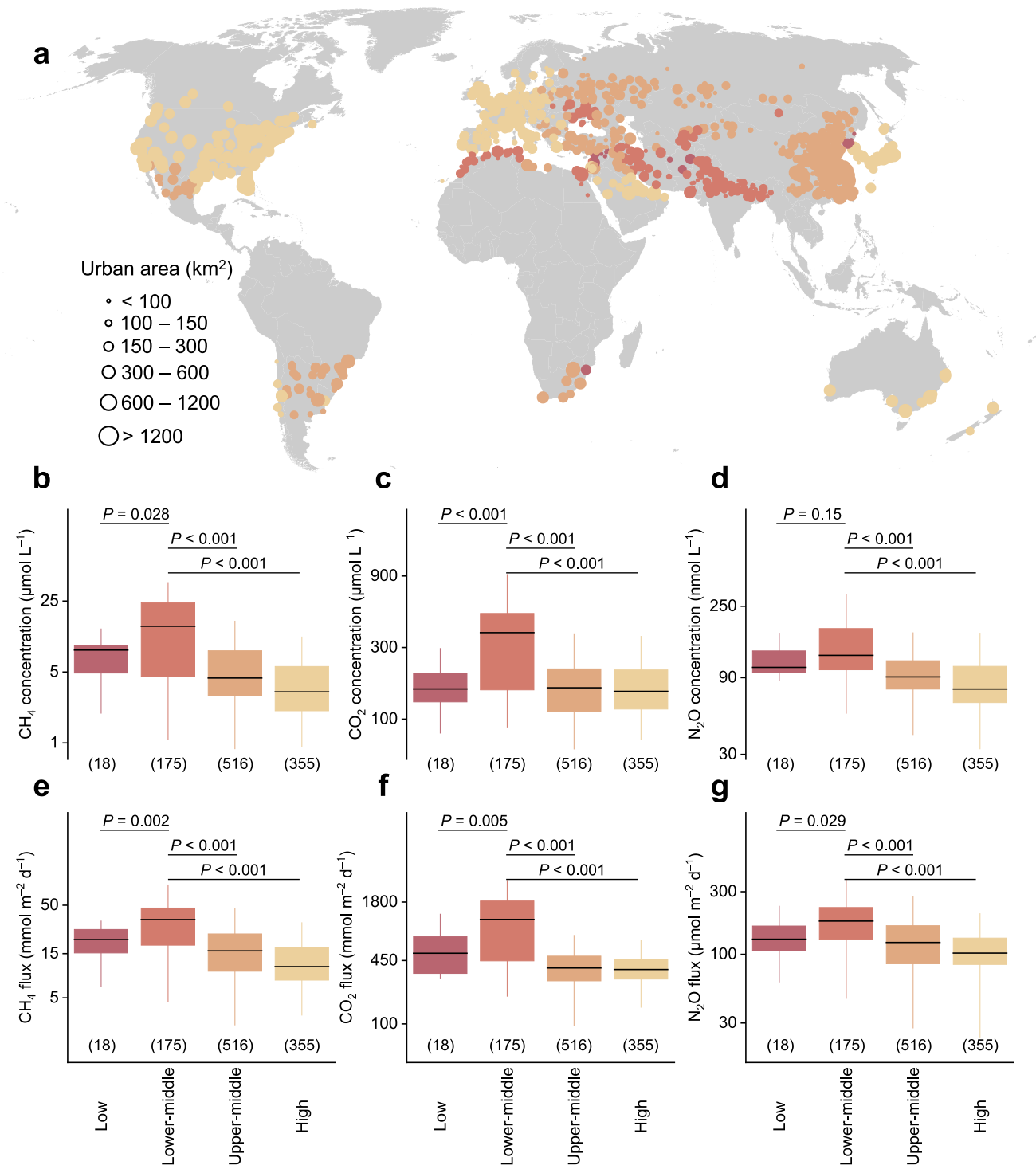
Dots represent individual data points, solid lines represent regression fits,

shaded areas are the 95% confidence intervals, number is the standardized regression coefficient \pm standard error. The *P* values were estimated with a two-sided *F*-test. No adjustments for multiple comparisons were made.



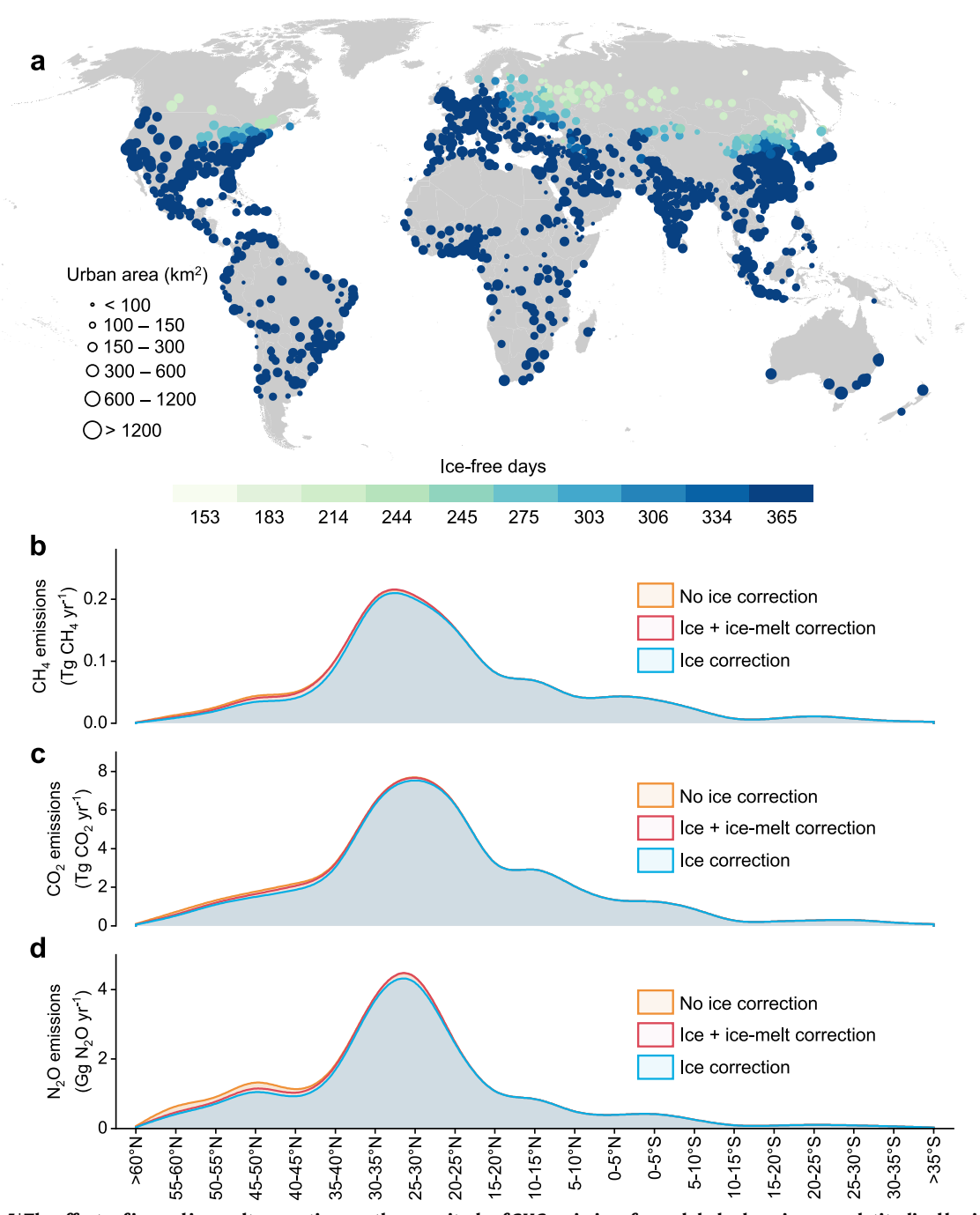
Extended Data Fig. 3 | Variable importance and model performance of GHG concentrations and fluxes. Mean decrease in accuracy (increase in mean squared error, %IncMSE) estimated from RF models and the model performance

on the 15% testing sub-dataset. ${\bf a,b}$, ${\rm CH_4}$. ${\bf c,d}$, ${\rm CO_2}$. ${\bf e,f}$, ${\rm N_2O}$. Dashed line represents the 1:1 line. ${\rm R^2}$ is the coefficient of determination of the linear regression and RMSE is the root mean square error.

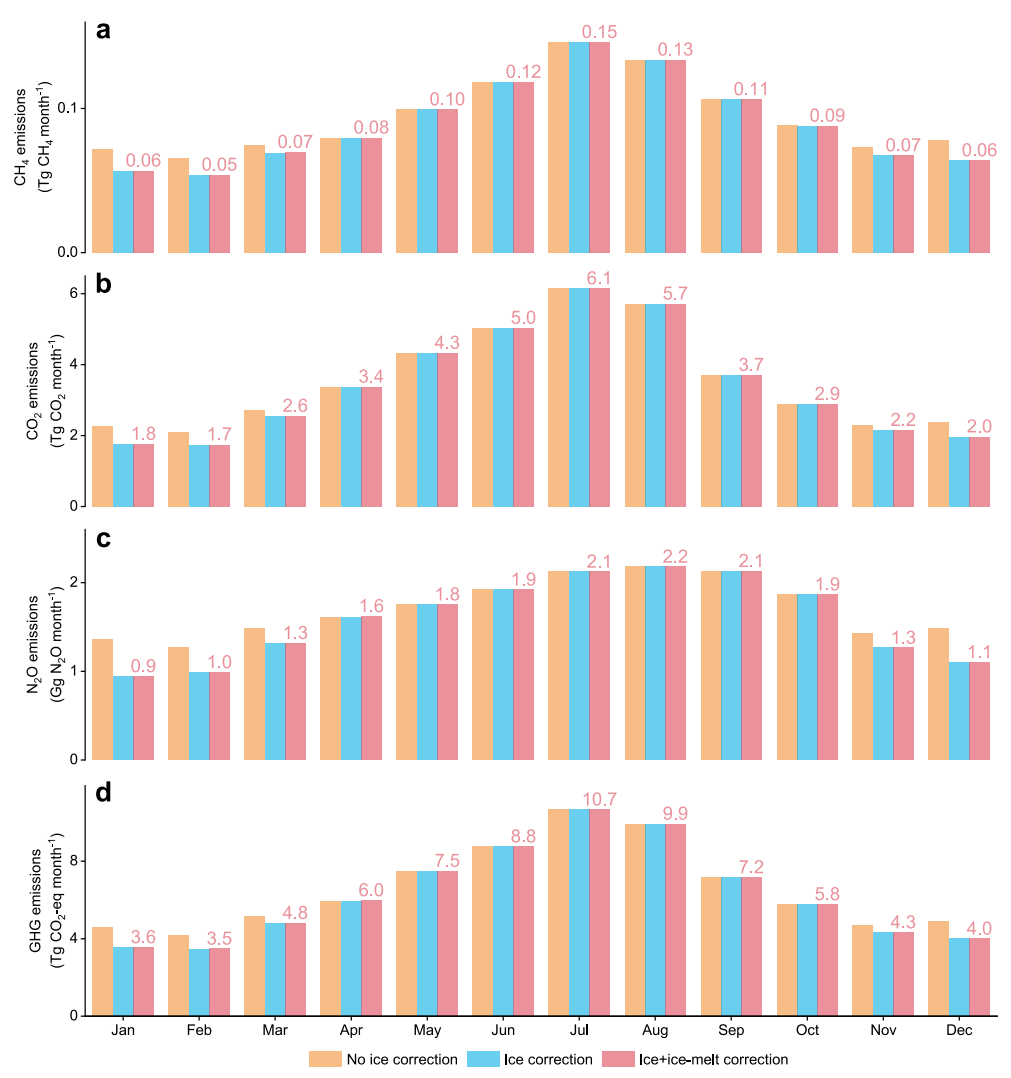


Extended Data Fig. 4 | Spatial variation of urban river GHG concentrations and fluxes across four income levels of temperate cities. a, Geographical distributions of temperate cities classified by four income levels. \mathbf{b} - \mathbf{g} , Boxplots show urban river GHG concentrations (\mathbf{b} - \mathbf{d}) and fluxes (\mathbf{e} - \mathbf{g}) in urban rivers of temperate cities. In each plot in \mathbf{b} - \mathbf{g} , box spans the 25th and 75th percentiles.

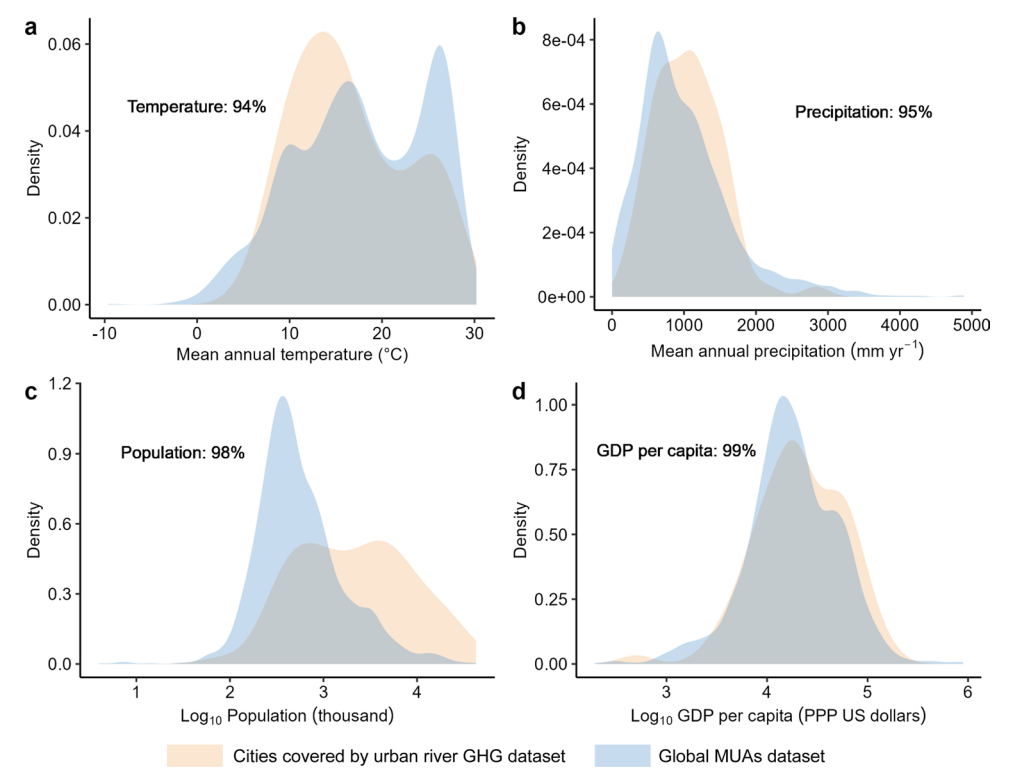
Solid line denotes the median and the whiskers represent 1.5 \times the interquartile range. Statistical significance between groups was tested with the two-sided Wilcoxon rank-sum test, using lower-middle as the reference group. Number in parentheses indicates number of measurements. Basemap in a from GADM (https://gadm.org/).



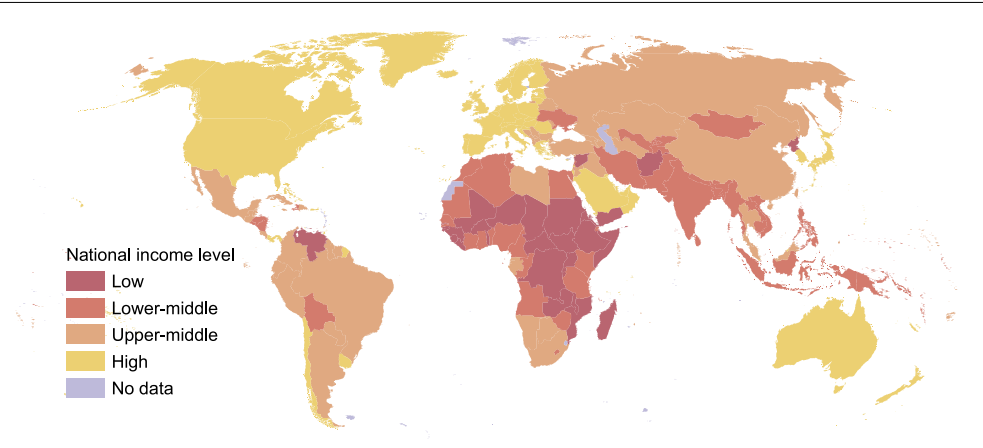
Extended Data Fig. 5 | The effects of ice and ice-melt corrections on the magnitude of GHG emissions from global urban rivers on a latitudinal basis. a, Annual ice-free days of urban rivers. \mathbf{b} - \mathbf{d} , The effects of ice and ice-melt correction on CH₄, CO₂, and N₂O emissions, respectively. Basemap in a from GADM (https://gadm.org/).



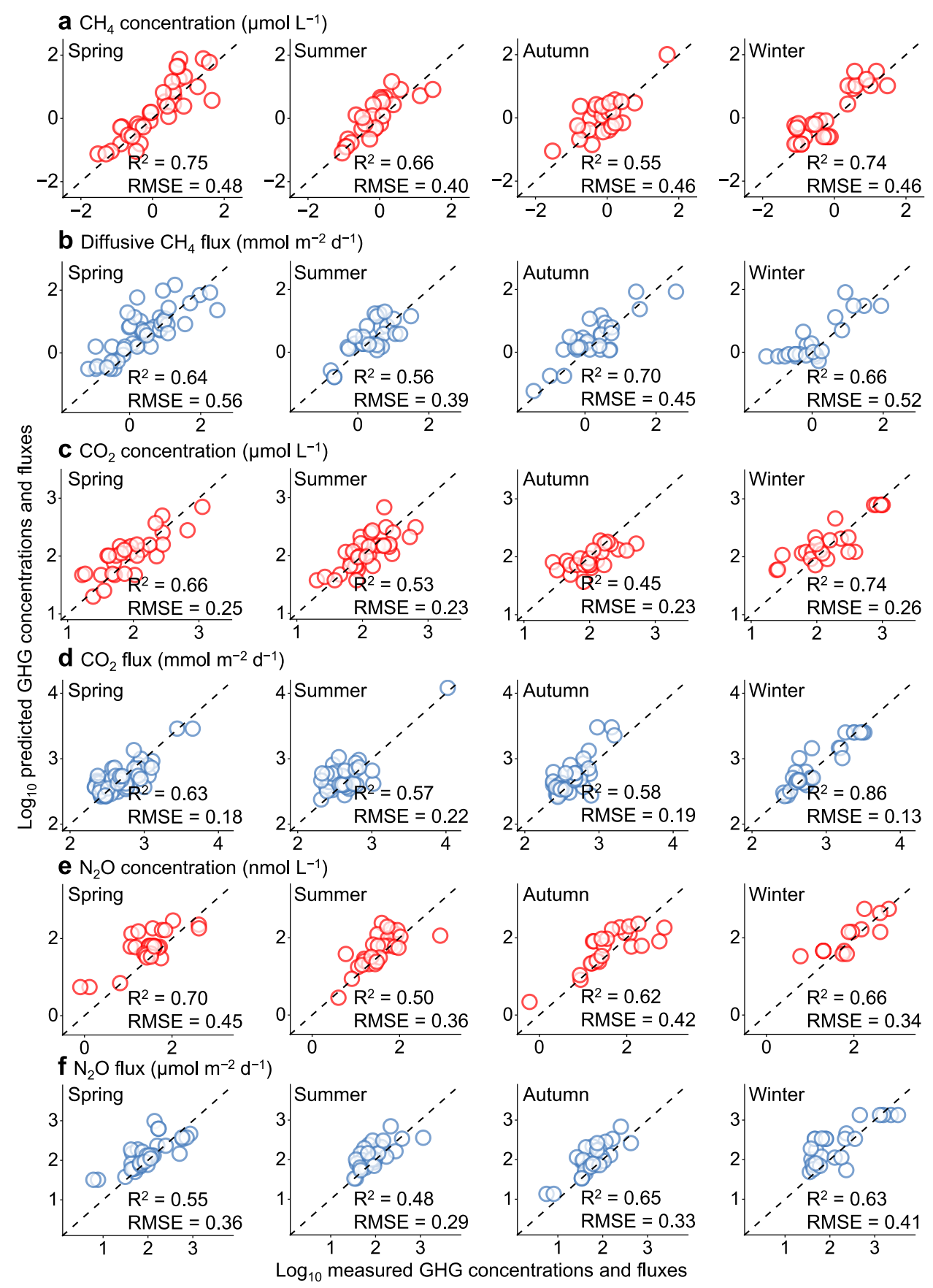
Extended Data Fig. 6 | Monthly variations of global urban river GHG emissions. a, CH_4 . b, CO_2 . c, N_2O . d, GHG in CO_2 -equivalent. Color-coded columns show the magnitude of changes in monthly emissions after applying the ice and ice-melt corrections.



Extended Data Fig. 7 | Major climatic and socioeconomic conditions of cities covered by the compiled urban river GHG dataset. a, Mean annual temperature. b, Mean annual precipitation. c, Log_{10} population. d, Log_{10} GDP per capita. Number in each subplot indicates the percentage of global MUAs covered by a corresponding parameter range from the urban river GHG dataset.



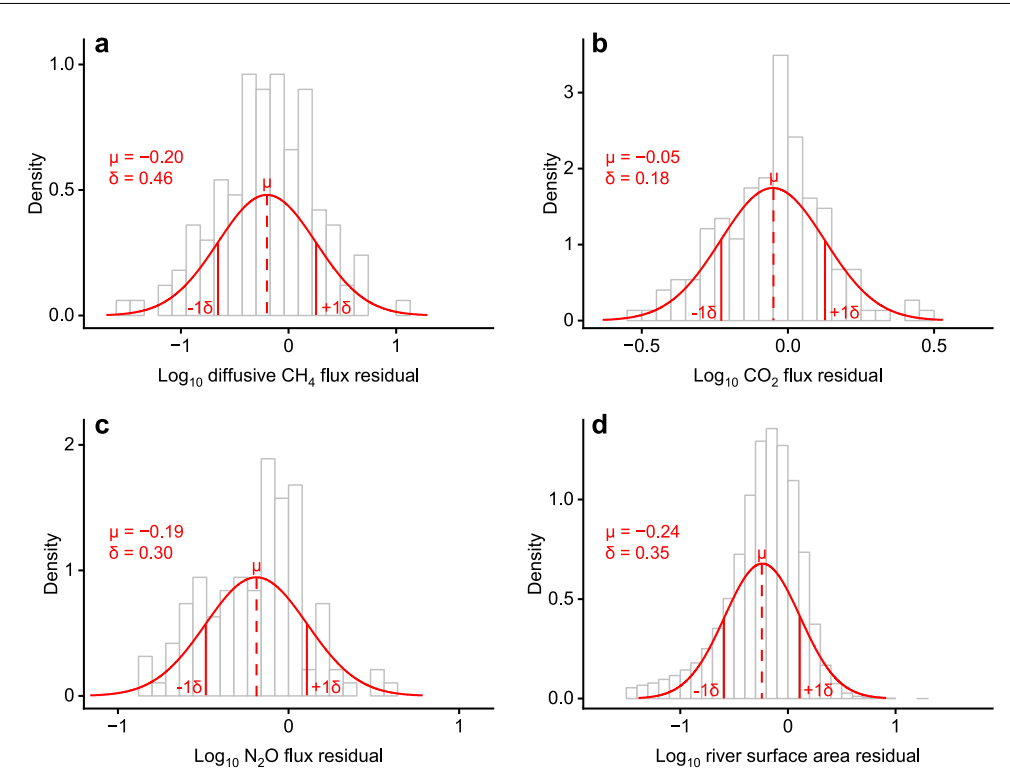
Extended Data Fig. 8 | Map showing national income level. Countries were classified into four groups based on gross national income per capita in 2021: low income countries (<\$1,085), lower-middle income countries (\$1,086-\$4,255), upper-middle income countries (\$4,256-\$13,205), and high income countries (>\$13,205). Basemap from GADM (https://gadm.org/).



Extended Data Fig. 9 | Model performance in separate seasons.

a-f, Comparisons between measured and predicted urban river GHG concentrations (**a**, **c**, **e**) and fluxes (**b**, **d**, **f**) values obtained from 15% testing

sub-set of RF model in separate seasons. **a,b**, CH_4 , **c,d**, CO_2 , **e,f**, N_2O . Dashed line represents the 1:1 line. R^2 is the coefficient of determination of the linear regression and RMSE is the root mean square error.



Extended Data Fig. 10 | Source of error for urban river GHG emission estimates. a-c, Flux errors from the RF modeling, which were determined by fitting the model residuals to a normal distribution and calculate the error at one

standard deviation (1δ) . **d**, Error associated with river surface area estimate in this analysis, which was determined by comparing with those from the Global River Width from Landsat (GRWL) Database.

nature portfolio

Corresponding author(s):	Shaoda Liu, Xinghui Xia
Last updated by author(s):	Apr 19, 2024

Reporting Summary

Nature Portfolio wishes to improve the reproducibility of the work that we publish. This form provides structure for consistency and transparency in reporting. For further information on Nature Portfolio policies, see our <u>Editorial Policies</u> and the <u>Editorial Policy Checklist</u>.

For all statistical analyses, confirm that the following items are present in the figure legend, table legend, main text, or Methods section.

<u> </u>				
St	·a:	t١	ς†	ics

n/a	Confirmed
	$oxed{oxed}$ The exact sample size (n) for each experimental group/condition, given as a discrete number and unit of measurement
	🔀 A statement on whether measurements were taken from distinct samples or whether the same sample was measured repeatedly
	The statistical test(s) used AND whether they are one- or two-sided Only common tests should be described solely by name; describe more complex techniques in the Methods section.
	A description of all covariates tested
	🔀 A description of any assumptions or corrections, such as tests of normality and adjustment for multiple comparisons
	A full description of the statistical parameters including central tendency (e.g. means) or other basic estimates (e.g. regression coefficient) AND variation (e.g. standard deviation) or associated estimates of uncertainty (e.g. confidence intervals)
	For null hypothesis testing, the test statistic (e.g. <i>F</i> , <i>t</i> , <i>r</i>) with confidence intervals, effect sizes, degrees of freedom and <i>P</i> value noted Give <i>P</i> values as exact values whenever suitable.
\boxtimes	For Bayesian analysis, information on the choice of priors and Markov chain Monte Carlo settings
\boxtimes	For hierarchical and complex designs, identification of the appropriate level for tests and full reporting of outcomes
\boxtimes	\square Estimates of effect sizes (e.g. Cohen's d , Pearson's r), indicating how they were calculated
	Our web collection on statistics for biologists contains articles on many of the points above.

Software and code

Policy information about availability of computer code

Data collection

Data of urban river greenhouse gas concentrations and fluxes and associated water physiochemical properties were either extracted directly from text and tables or estimated following the Fick's Law using local water physiochemical parameters as drivers. GetData Graph Digitizer (version 2.22) was used to extract data from figures. Reach-level catchment environmental and socioeconomic predictors were calculated by overlapping the catchments with relevant geospatial datasets using the mask tool of the Python Rasterio toolsets (version 1.4).

Data analysis

Data analysis was conducted with the software Microsoft Excel (version 2021), OriginPro (version 2023), randomForest package in R (version 4.2.1), and ArcGIS (version 10.8). The code used in this study is available from https://doi.org/10.6084/m9.figshare.24233902.

For manuscripts utilizing custom algorithms or software that are central to the research but not yet described in published literature, software must be made available to editors and reviewers. We strongly encourage code deposition in a community repository (e.g. GitHub). See the Nature Portfolio <u>guidelines for submitting code & software</u> for further information.

Data

Policy information about availability of data

All manuscripts must include a data availability statement. This statement should provide the following information, where applicable:

- Accession codes, unique identifiers, or web links for publicly available datasets
- A description of any restrictions on data availability
- For clinical datasets or third party data, please ensure that the statement adheres to our policy

The global morphological urban areas product is available from https://data.mendeley.com/datasets/v3p8gk5724/1. The Global Reach-scale A priori Discharge Estimates for SWOT (GRADES) dataset is available from https://www.reachhydro.org/home/records/grades. The Global River Methane Database (GriMeDB) is available from https://doi.org/10.6073/pasta/f48cdb77282598052349e969920356ef. The temperature and precipitation are available from WorldClim (version 2) (https://www.worldclim.org/data/worldclim21.html). The elevation and slope are available from Global Multi-resolution Terrain Elevation Dataset (https://www.earthenv.org/topography). The GDP and GDP per capita are available from Gridded global datasets for Gross Domestic Product and Human Development Index over 1990-2015 (https://datadryad.org/stash/dataset/doi:10.5061/dryad.dk1j0). The population density is available from Gridded Population of the World (version 4) (https://beta.sedac.ciesin.columbia.edu/data/set/gpw-v4-population-density). The MODIS gross and net primary productivity data are available from https://www.umt.edu/numerical-terradynamic-simulation-group/project/modis/mod17.php. The soil respiration rates data is available from http://cse.ffpri.affrc.go.jp/shojih/data/index.html. Detailed information on a array of spatially explicit geospatial datasets used in this analysis is summarized in Supplementary Table 4. The dataset of urban river GHG concentrations and fluxes and related physiochemical properties is available from https://doi.org/10.6084/m9.figshare.24233902. Source data are provided with this paper.

		1	4.5	
Н	IIMan	research	narticii	nantc
	ulliali	I C3Cal CII	pai titij	Janto

Policy information about <u>studies involving human research participants and Sex and Gender in Research.</u>				
Reporting on sex and gender	N/A			
Population characteristics	N/A			
Recruitment	N/A			
Ethics oversight	N/A			
Note that full information on the approval of the study protocol must also be provided in the manuscript.				
Field-specific reporting				
Please select the one below that is the best fit for your research. If you are not sure, read the appropriate sections before making your selection.				
Life sciences	Behavioural & social sciences 🔀 Ecological, evolutionary & environmental sciences			
For a reference copy of the document wit	h all sections, see <u>nature.com/documents/nr-reporting-summary-flat.pdf</u>			

Ecological, evolutionary & environmental sciences study design

All studies must disclose on these points even when the disclosure is negative.

Study description

In this analysis, we aim to identify unique greenhouse gas emission profiles from global urban rivers, the environmental and socioeconomic drivers for their patterns and implications of the emissions. In order to achieve these goals, we compiled a data involving as many measurements of greenhouse gas concentrations/fluxes in urban rivers from the published literature. We then first reviewed present urban river greenhouse gas measurements in the literature and pointed out distinctive greenhouse gas emission profiles (e.g., particularly higher CH4 and N2O emissions) from urban than in non-urban rivers. Then, relying on a machine learning-based algorithm, we established predictive models between urban river greenhouse gas emissions and a range of reach-level catchment environmental and socioeconomic drivers, which allowed us to extrapolate our results to the global scale. These results finally allowed us a quantitative assessment of greenhouse emissions from global urban rivers, their geographic patterns, socioeconomic drivers and implications.

Research sample

The dataset of urban river greenhouse gas concentrations and fluxes was compiled from 116 published literature and contained 829, 809, and 644 for CO2, CH4, and N2O concentrations, respectively; and 1,034, 914, 860 for CO2, CH4, and N2O fluxes, respectively. Prediction of greenhouse gas emissions from urban rivers cover 1,554 global morphological urban areas.

Sampling strategy

Sampling strategy is not relevant to our study. All data were from published literature and open datasets.

Data collection

All data are from published literature and open datasets.

Timing and spatial scale

Data were compiled from the literature published between 1999 and 2023. Data includes greenhouse gas measurements in urban

_
ب
าลเน
_ =
ē
(D
$\neg \neg$
\simeq
\sim
_
\neg
==
\circ
TOIIC
\circ
_
\overline{A}
Te
rep
repo
repo
repor
reporti
reportin
ă
ă
reporting
ă
ă
ă
ă
ă
ă
ă
ă

Timing and spatial scale	(rivers in Asia, Africa, Europe, North and South America and Oceania.	
Data exclusions	We retained only studies that report in situ measurements of urban river GHG concentrations or fluxes. For studies that have measurements from both urban and non-urban river segments, all sites were retained for comparative analysis. We also kept the database strictly spatially explicit so that exact geographic locations of the measurement sites can be determined.	
Reproducibility	Results can be reproduced following the data and methods described in the manuscript.	
Randomization	Data were randomly split for training and testing of the random forest models.	
Blinding	Blinding is not relevant to this study. All data were from published literature and open datasets.	
Did the study involve field work? Yes No		

Reporting for specific materials, systems and methods

We require information from authors about some types of materials, experimental systems and methods used in many studies. Here, indicate whether each material, system or method listed is relevant to your study. If you are not sure if a list item applies to your research, read the appropriate section before selecting a response.

Materials & experimental systems		Methods	
n/a	Involved in the study	n/a Involved in the study	
\boxtimes	Antibodies	ChIP-seq	
\boxtimes	Eukaryotic cell lines	Flow cytometry	
\boxtimes	Palaeontology and archaeology	MRI-based neuroimaging	
\boxtimes	Animals and other organisms		
\boxtimes	Clinical data		
\boxtimes	Dual use research of concern		